Titre: Title:	A finite line source simulation model for geothermal systems with series- and parallel-connected boreholes and independent fluid loops
Auteurs: Authors:	Massimo Cimmino
Date:	2018
Type:	Article de revue / Article
Référence: Citation:	Cimmino, M. (2018). A finite line source simulation model for geothermal systems with series- and parallel-connected boreholes and independent fluid loops. Journal of Building Performance Simulation, 11 (4), 414-432. https://doi.org/10.1080/19401493.2017.1381993

Titre de la revue: Journal Title:	Journal of Building Performance Simulation (vol. 11, no. 4)
Maison d'édition: Publisher:	Taylor & Francis
URL officiel: Official URL:	https://doi.org/10.1080/19401493.2017.1381993
Mention légale: Legal notice:	This is an Accepted Manuscript of an article published by Taylor & Francis in Journal of Building Performance Simulation (vol. 11, no. 4) in 2018, available online: https://doi.org/10.1080/19401493.2017.1381993

A finite line source simulation model for geothermal systems with series and parallel connected boreholes and independent fluid loops

Massimo Cimmino

Département de génie mécanique, Polytechnique Montréal, Montréal, Canada

Département de génie mécanique
Polytechnique Montréal
Case Postale 6079, succursale "centre-ville"
Montreal, Quebec, Canada, H3C 3A7
massimo.cimmino@polymtl.ca

A finite line source simulation model for geothermal systems with series and parallel connected boreholes and independent fluid loops

A model for the simulation of geothermal systems with parallel- and series-connected boreholes is presented. Mass and heat balance problems are formulated for each component in the system and are assembled into system-level problems. A third problem is formulated to account for heat transfer in the bore field, using the finite line source solution. This third problem is coupled to the system-level heat balance problem by an analytical solution of the heat transfer inside boreholes with multiple U-tubes. The simulation model allows for any number of independent fluid loops within the bore field or within individual boreholes and allows for combinations of specified inlet fluid temperatures and heat extraction rates in independent fluid loops. The model accounts for the axial variation of the fluid and borehole wall temperatures and heat extraction rates. The capabilities of the model are demonstrated through three example simulations.

Keywords: Geothermal boreholes; Ground heat exchangers; Parallel arrangement; Series arrangement; Multiple U-tubes; Thermal response factors

Nomenclature

Variables

α_s	Soil thermal diffusivity
Δt	Simulation time step
Δt_p	Size of aggregation cell p
ΔT_b	Borehole wall temperature drop
c_p	Specific heat capacity
COP	Heat pump coefficient of performance
d	Distance between boreholes
D	Borehole or borehole segment buried depth
ε_{abs,T_b}	Absolute error tolerance on borehole wall temperatures
ε_{abs,T_f}	Absolute error tolerance on fluid temperatures
$\varepsilon_{rel,\dot{m}_f}$	Relative error tolerance on fluid mass flow rates
G	Captured solar radiation
h	Segment-to-segment thermal response factor
H	Borehole or borehole segment length
k_s	Ground thermal conductivity
$\dot{m}_{f,in}$	Inlet fluid mass flow rate
$\dot{m}_{f,out}$	Outlet fluid mass flow rate
η	Solar collector efficiency
N_{agg}	Total number of load aggregation cells
N_b	Total number of boreholes in bore field
N_c	Total number of system components
n_{in}	Number of inlets in component
N_{in}	Total number of inlets in system
n_{out}	Number of outlets in component
N_{out}	Total number of outlets in system
n_p	Number of U-tubes in borehole
N_p	Total number of U-tubes in bore field

n_q	Number of borehole segments in borehole
N_q	Total number of borehole segments in bore field
$\dot{Q}$	Component heat transfer rate
$\dot{Q}_b$	Borehole heat extraction rate
$\dot{Q}_{building}$	Building load
$\dot{Q}_p$	Pipe heat transfer rate
r_b	Borehole radius
R^{Δ}	Delta-circuit thermal resistance
R_b^*	Effective borehole thermal resistance
R_{fp}	Fluid to outer pipe wall thermal resistance
$r_{p,in}$	Pipe inner radius
$r_{p,out}$	Pipe outer radius
t	Time
T_a	Ambient temperature
T_b	Borehole wall temperature
T_f	Fluid temperature in borehole pipes
$T_{f,in}$	Inlet fluid temperature
$T_{f,out}$	Outlet fluid temperature
T_g	Undisturbed ground temperature
(x, y)	Coordinates of boreholes or pipes
z	Depth

Matrices and vectors

$\boldsymbol{A}$	Coefficient matrix of the system of differential equations for fluid temperatures in boreholes
$\boldsymbol{a}_{\dot{m}_f}$	Coefficient matrix for the component-level mass balance problem
$\boldsymbol{A}_{\dot{m}_f}$	Coefficient matrix for the system-level mass balance problem
$\boldsymbol{a}_{Q_b}$	Coefficient matrix for the borehole heat transfer problem
$\boldsymbol{A}_{Q_b}$	Coefficient matrix for the bore field heat transfer problem

$\boldsymbol{a_{T_f}}$ Coefficient matrix for the component-level heat balance problem

$\boldsymbol{A_{T_f}}$ Coefficient matrix for the system-level heat balance problem

$\boldsymbol{b_{\dot{m}_f}}$ Coefficient vector for the component-level mass balance problem

$\boldsymbol{B_{\dot{m}_f}}$ Coefficient vector for the system-level mass balance problem

$\boldsymbol{b_{Q_b}}$ Coefficient vector for the borehole heat transfer problem

$\boldsymbol{B_{Q_b}}$ Coefficient vector for the bore field heat transfer problem

$\boldsymbol{b_{T_f}}$ Coefficient vector for the component-level heat balance problem

$\boldsymbol{B_{T_f}}$ Coefficient vector for the system-level heat balance problem

$\boldsymbol{C}$ Component connectivity matrix

$\boldsymbol{E}$ Matrix exponential of $\boldsymbol{A}z$

$\boldsymbol{E_{in}}$, $\boldsymbol{E_{out}}$, $\boldsymbol{E_b}$ Coefficient matrices for boundary condition at $z = H$

$\boldsymbol{H}$ Matrix of segment-to-segment thermal response factors

$\boldsymbol{I}$ Identity matrix

$\boldsymbol{L}$ Diagonal matrix of eigenvalues of $\boldsymbol{A}$

$\boldsymbol{\dot{m}_{f,in}}$ Vector of inlet fluid mass flow rates

$\boldsymbol{\dot{m}_{f,out}}$ Vector of outlet fluid mass flow rates

$\boldsymbol{\dot{Q}_b}$ Vector of heat extraction rate per unit length of borehole segments

$\boldsymbol{T_b}$ Vector of average borehole segment temperatures

$\boldsymbol{T_{b,0}}$ Vector of average borehole segment temperatures assuming no heat extraction during current time step

$\boldsymbol{T_{f,in}}$ Vector of inlet fluid temperatures

$\boldsymbol{T_{f,out}}$ Vector of outlet fluid temperatures

$\boldsymbol{T_f}$ Vector of fluid temperatures in borehole pipes

$\boldsymbol{T_g}$ Vector of undisturbed ground temperatures

$\boldsymbol{V}$ Matrix of eigenvectors of $\boldsymbol{A}$

$\boldsymbol{y}$ Vector of mass flow rate fractions

Indices

i_b, j_b Borehole indices

i_c, j_c	Component indices
i_p, j_p	Pipe indices
k	Time index
$specified$	Specified value of the variable
tot	Total value in the bore field
u, v	Borehole segment indices

1. Introduction

In heating dominated applications, ground source heat pump (GSHP) systems extract a greater amount of heat during the heating season than they inject heat back into the ground during the cooling season. Because of this load imbalance, the thermal efficiency of a GSHP system will degrade over the years as the ground temperature decreases. Design methods for vertical borehole fields aim to identify the required length of boreholes that is necessary to keep the heat carrier fluid above a lower temperature limit. A GSHP system with unbalanced loads will typically require longer boreholes than a GSHP system with balanced loads.

Thermal energy storage from an auxiliary source (e.g. solar collectors or industrial waste heat) has been proposed to counteract the effects of load imbalance and reduce the required borehole length. Different strategies of heat storage and extraction in borehole fields have been considered: (1) reversal of flow direction in fields of boreholes connected in series during storage and extraction periods (Cui et al. 2015), (2) storage and extraction of thermal energy in independent clusters of boreholes (Monzó et al. 2013; Belzile, Lamarche, and Rousse 2016a), and (3) storage and extraction of heat in independent U-tubes within the boreholes (Eslami-nejad and Bernier 2011; Cimmino and Eslami-Nejad 2016; Belzile, Lamarche, and Rousse 2016b).

Simulation of GSHP systems is often conducted using thermal response factors. Eskilson (Eskilson 1987) first introduced numerical thermal response factors, or g-functions, for the

simulation of fields of geothermal boreholes connected in parallel. Zeng et al. (Zeng, Diao, and Fang 2002) proposed the spatial superposition of the finite line source (FLS) analytical solution to estimate g-functions, and Larmache and Beauchamp (Lamarche and Beauchamp 2007) and Claesson and Javed (Claesson and Javed 2011) gave simplified formulations of the analytical solution. By dividing boreholes into series of finite line source segments, Cimmino and Bernier (Cimmino and Bernier 2014) and Lazzarotto and Björk (Lazzarotto 2016; Lazzarotto and Björk 2016) obtained accurate evaluations of the g-functions for vertical and tilted boreholes. Their method allowed the axial variation of the heat extraction rates along the boreholes and the evaluation of g-functions that approach a condition of uniform borehole wall temperatures, as done by Eskilson using a finite difference method. Extensions to the finite line source method for the evaluation of thermal response factors have also been proposed for mixed series-parallel configurations (Marcotte and Pasquier 2014) and for a condition of equal inlet fluid temperature into the bore field (Cimmino 2015).

The g-function method relies on the assumption of constant fluid flow rate and direction of flow through the boreholes, and that all boreholes are connected to a single inlet fluid stream. It is therefore inadequate in modelling bore fields with independently connected clusters of boreholes or with multiple independent fluid loops. To overcome these shortcomings, numerical methods are useful to simulate geothermal systems and take into account more complex phenomena; for example groundwater advection (Nguyen, Pasquier, and Marcotte 2017), variable fluid flow rate (Zarrella, Emmi, and De Carli 2017) and short-term heat transfer inside the boreholes (Bauer, Heidemann, and Diersch 2011). However, numerical methods are generally computationally expensive when compared to analytical methods with appropriate load aggregation schemes (Bernier et al. 2004; Liu 2005; Lamarche 2009; Claesson and Javed 2012).

Numerical methods can thus be impractical for the simulation of very large bore fields or for the design optimization of geothermal systems.

A network-based methodology was proposed by Lazzarotto (Lazzarotto 2014; Lazzarotto 2015), and recently extended by Lamarche (Lamarche 2017), using the finite line source solution to model geothermal boreholes. This methodology enables the simulation of arbitrarily positioned and connected boreholes. It integrates models for the various system components found in geothermal systems (e.g. pumps, heat exchangers and pipe manifolds). Two sets of problems for mass and heat balance are formulated at the component level and assembled into global mass and heat balance problems at the system level. The system-level heat balance problem includes all model variables from system components, such as borehole wall temperatures and heat fluxes in the finite line source method used to model boreholes. However, the methodology does not account for the axial variations of the heat extraction rates and of the fluid and borehole wall along the boreholes.

This paper proposes an improved methodology for the simulation of geothermal systems. As done by Lazzarotto (Lazzarotto 2014; Lazzarotto 2015), mass and heat balance problems are formulated at the component level and assembled into system-level systems of equations. A third problem is introduced to account for heat transfer in the field of geothermal boreholes. Borehole-type system components are thus used both in the formulation of the system-level heat balance problem and in the bore field heat transfer problem. The three problems, i.e. system-level (1) mass and (2) heat balance and (3) bore field heat transfer, are solved successively in an iterative process at each time step of the simulations. The improved methodology accounts for the axial variation of temperatures and heat extraction rates along the boreholes and allows for the simulation of bore fields with boreholes of unequal lengths.

2. Mathematical model

Figure 1 shows a geothermal bore field with two independent fluid loops running in counter flow in four parallel branches of four series-connected boreholes. To simulate the performance of such geothermal systems with complex fluid network topology, the proposed methodology separates the system into two distinct regions: (1) the fluid side and (2) the ground side. The borehole walls act as an interface between the two regions.

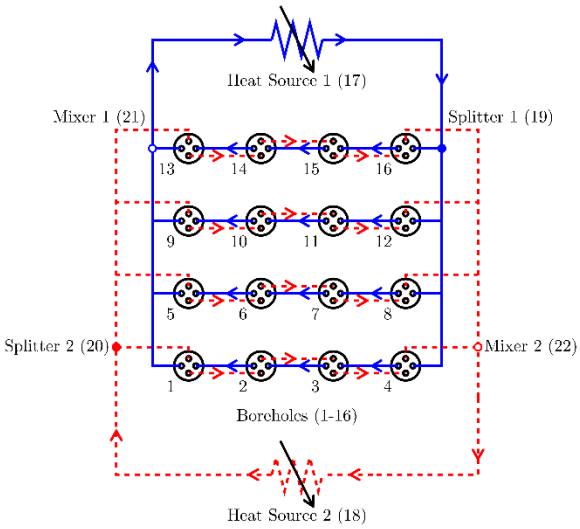

Figure 1. Field of 16 boreholes with two independent fluid loops

On the fluid side, the system is further divided into its component parts, and each system component is modelled separately from the other components. For example, in Figure 1, the system includes 16 boreholes (1-16), two heat sources (17-18), two flow splitters (19-20) and two flow mixers (21-22). Only two flow splitters are shown on Figure 1 rather than four on each side. The proposed methodology does not explicitly account for head losses in pipes to distribute flow between branches. Flow fractions exiting each branch of a splitter component are specified and thus having one splitter on each side is equivalent to having four in the example shown on Figure 1. Mass and heat balance problems are formulated for each of the components in the form

of matrix systems of equations. These component-level problems are cast as matrix systems of linear equations involving inlet and outlet mass flow rates and fluid temperatures, regardless of the type of component. The component-level problems are assembled into system-level – or global – mass and heat transfer problems, considering the connections between the components.

On the ground side, boreholes are modelled as series of finite line heat sources. A bore field heat transfer problem is constructed from the spatial and temporal superposition of the finite line source analytical solution, considering the variation (spatial and temporal) of the heat extraction rates in the bore field. Boreholes are the only components shared by the fluid-side problems and the bore field heat transfer problem. In the proposed methodology, an analytical solution of the thermal interactions between U-tube pipes and between U-tube pipes and the borehole wall is used to couple the problems in the two regions.

The structure of the mathematical model is presented in Figure 2. For each system component, component-level coefficient matrices and vectors for the mass ($\boldsymbol{a}_{\dot{m}_f}$ and $\boldsymbol{b}_{\dot{m}_f}$) and heat balance ($\boldsymbol{a}_{T_f}$ and $\boldsymbol{b}_{T_f}$) problems are assembled into the system-level mass and heat transfer problems. The solution to these problems returns the inlet and outlet mass flow rates and fluid temperatures. From these evaluated values, coefficient matrices and vectors ($\boldsymbol{a}_{Q_b}$ and $\boldsymbol{b}_{Q_b}$) are assembled into the bore field heat transfer problem. The solution to this third problem returns the borehole wall temperatures and heat extraction rates. In cases where fluid temperatures or mass flow rates are dependent on borehole wall temperatures (and vice-versa), the solution to all three problems are obtained from the successive solution of each problem until the evaluated mass flow rates, fluid temperatures and borehole wall temperatures converge to their final values.

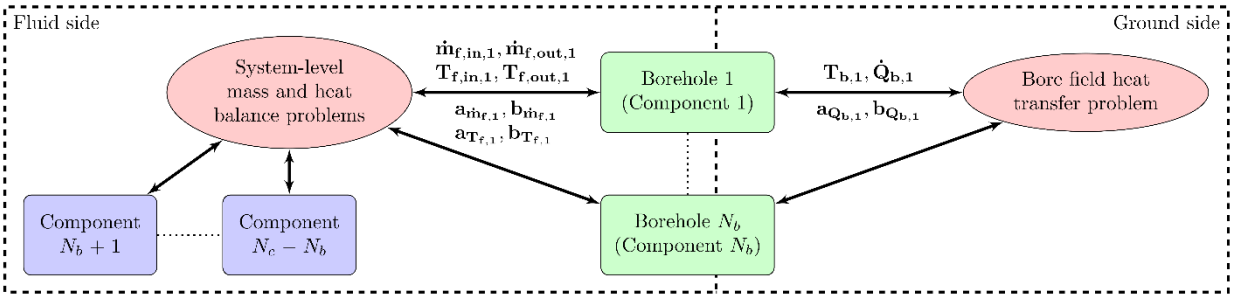

Figure 2. Structure of the presented mathematical model

2.1. Component-level mass and heat balance problems

For each component in the system, the mass and heat balance problems are formulated as linear systems of equations between inlet and outlet mass flow rates and between inlet and outlet fluid temperatures, respectively. For an arbitrary component i_c with n_{in,i_c} fluid inlets and n_{out,i_c} fluid outlets, the component-level mass and heat balance problems may be cast in the linear form:

$$\boldsymbol{\dot{m}_{f,out,i_c}} = \boldsymbol{a_{\dot{m}_{f,i_c}}} \boldsymbol{\dot{m}_{f,in,i_c}} + \boldsymbol{b_{\dot{m}_{f,i_c}}} \tag{1}$$

$$\boldsymbol{T_{f,out,i_c}} = \boldsymbol{a_{T_{f,i_c}}} \boldsymbol{T_{f,in,i_c}} + \boldsymbol{b_{T_{f,i_c}}} \tag{2}$$

where $\boldsymbol{\dot{m}_{f,in,i_c}}$ is a $n_{in,i_c} \times 1$ column vector of inlet fluid mass flow rates into the component, $\boldsymbol{\dot{m}_{f,out,i_c}}$ is a $n_{out,i_c} \times 1$ column vector of outlet fluid mass flow rates out of the component, $\boldsymbol{T_{f,in,i_c}}$ is a $n_{in,i_c} \times 1$ column vector of inlet fluid temperatures into the component, $\boldsymbol{T_{f,out,i_c}}$ is a $n_{out,i_c} \times 1$ column vector of outlet fluid temperatures out of the component, $\boldsymbol{a_{T_{f,i_c}}}$ and $\boldsymbol{a_{\dot{m}_{f,i_c}}}$ are $n_{out,i_c} \times n_{in,i_c}$ coefficient matrices for the mass and heat balance problems, respectively, and $\boldsymbol{b_{T_{f,i_c}}}$ and $\boldsymbol{b_{\dot{m}_{f,i_c}}}$ are $n_{out,i_c} \times 1$ coefficient vectors for the mass and heat balance problems, respectively.

The coefficient matrices and vectors are obtained from physical models of the corresponding component i_c. In the present work, analytical system component models, which can easily be expressed in linear form as in Equations (1) and (2), are used. In some cases, the coefficient matrices and vectors are themselves dependent on the fluid temperatures, mass flow rates or other variables relevant to the component. In these cases, coefficient matrices and vectors are recalculated every time step or every iteration within each time step, as needed. The proposed framework does not prevent the use of numerical models for system components as long as the mass and heat balance problems in the form of Equations (1) and (2) may be formulated based on the current state of the system component.

Basic models for system components are described in this section. In addition to components previously shown on Figure 1, fluid sources and sinks are introduced to deal with conditions of prescribed inlet temperatures into fluid loops, rather than the prescribed heat transfer rates covered by the heat source components.

2.1.1. Fluid source and sink

The fluid source component supplies fluid at a specified temperature and mass flow rate and serves as a starting point to an open fluid loop, as shown on Figure 3. This component has no fluid inlets ($n_{in,i_c} = 0$) and only one fluid outlet ($n_{out,i_c} = 1$). The coefficient matrices and vectors for this component are given by:

$$\boldsymbol{a}_{\dot{\boldsymbol{m}}_{\boldsymbol{f},\boldsymbol{i_c}}} = [\quad] \tag{3}$$

$$\boldsymbol{b}_{\dot{\boldsymbol{m}}_{\boldsymbol{f},\boldsymbol{i_c}}} = \dot{m}_{f,out,i_c,specified} \tag{4}$$

$$\boldsymbol{a}_{\boldsymbol{T}_{\boldsymbol{f},\boldsymbol{i_c}}} = [\quad] \tag{5}$$

$$\boldsymbol{b}_{\boldsymbol{T}_{f,i_c}} = T_{f,out,i_c,specified} \tag{6}$$

where $\dot{m}_{f,out,i_c,specified}$ and $T_{f,out,i_c,specified}$ are the specified mass flow rate and fluid temperature out of the fluid source. [ ] denotes an empty coefficient matrix and simply means that these matrices are not used since a fluid source has no inlet ($n_{in,i_c} = 0$).

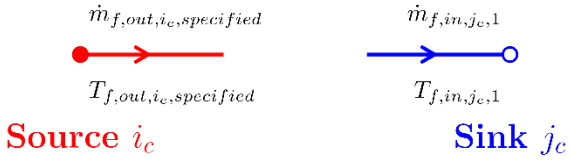

Figure 3. Fluid source and sink system components

The fluid sink component serves as an end point to an open fluid loop, as shown on Figure 3. This component has only one fluid inlet ($n_{in,j_c} = 1$) and no fluid outlets ($n_{out,j_c} = 0$). The coefficient matrices and vectors for this component are:

$$\boldsymbol{a}_{\dot{\boldsymbol{m}}_{\boldsymbol{f},\boldsymbol{j_c}}} = [\ \ ] \tag{7}$$

$$\boldsymbol{b}_{\dot{\boldsymbol{m}}_{\boldsymbol{f},\boldsymbol{j_c}}} = [\ \ ] \tag{8}$$

$$\boldsymbol{a}_{\boldsymbol{T}_{\boldsymbol{f},\boldsymbol{j_c}}} = [\ \ ] \tag{9}$$

$$\boldsymbol{b}_{\boldsymbol{T}_{\boldsymbol{f},\boldsymbol{j_c}}} = [\ \ ] \tag{10}$$

All coefficient matrices and vectors of the fluid sink are empty. While this component is not necessary to evaluate fluid temperatures and mass flow rates in the global system, it is useful in the verification of connections between components and ensures that the total number of component fluid inlets in the global system is equal to the total number of component fluid outlets.

2.1.2. Flow splitter and mixer

The flow splitter component splits a single fluid stream ($n_{in,i_c} = 1$) into a given number n_{out,i_c} of outlet fluid streams with specified ratios of the inlet mass flow rate, as shown on Figure 4. The outlet fluid temperatures of the flow splitter are equal to the inlet fluid temperature into the splitter. The coefficient matrices and vectors for this component are given by:

$$\boldsymbol{a}_{\dot{\boldsymbol{m}}_{f,i_c}} = \boldsymbol{y}_{\boldsymbol{i_c}} \tag{11}$$

$$\boldsymbol{b}_{\dot{\boldsymbol{m}}_{f,i_c}} = \mathbf{0}_{n_{out,i_c}\times 1} \tag{12}$$

$$\boldsymbol{a}_{\boldsymbol{T}_{f,i_c}} = \mathbf{1}_{n_{out,i_c}\times 1} \tag{13}$$

$$\boldsymbol{b}_{\boldsymbol{T}_{f,i_c}} = \mathbf{0}_{n_{out,i_c}\times 1} \tag{14}$$

where $\boldsymbol{y}_{\boldsymbol{i_c}}$ is a $n_{out,i_c} \times 1$ column vector of the outlet mass flow rate fractions relative to the inlet mass flow rate (see Figure 4), $\mathbf{0}_{m\times \mathrm{n}}$ is an $m \times n$ matrix of zeros and $\mathbf{1}_{m\times \mathrm{n}}$ is an $m \times n$ matrix of ones. Note that the sum of mass flow rate fractions $\mathbf{1}_{1\times n_{out,i_c}}\boldsymbol{y}_{\boldsymbol{i_c}}$ must be equal to 1 to ensure conservation of mass. Since head losses are not calculated in the proposed methodology, the flow distribution at the outlet of flow splitter components are assumed to be known. In the case the flow distribution is not known, mass flow rates should be calculated in a separate model and used to evaluate $\boldsymbol{y}_{\boldsymbol{i_c}}$.

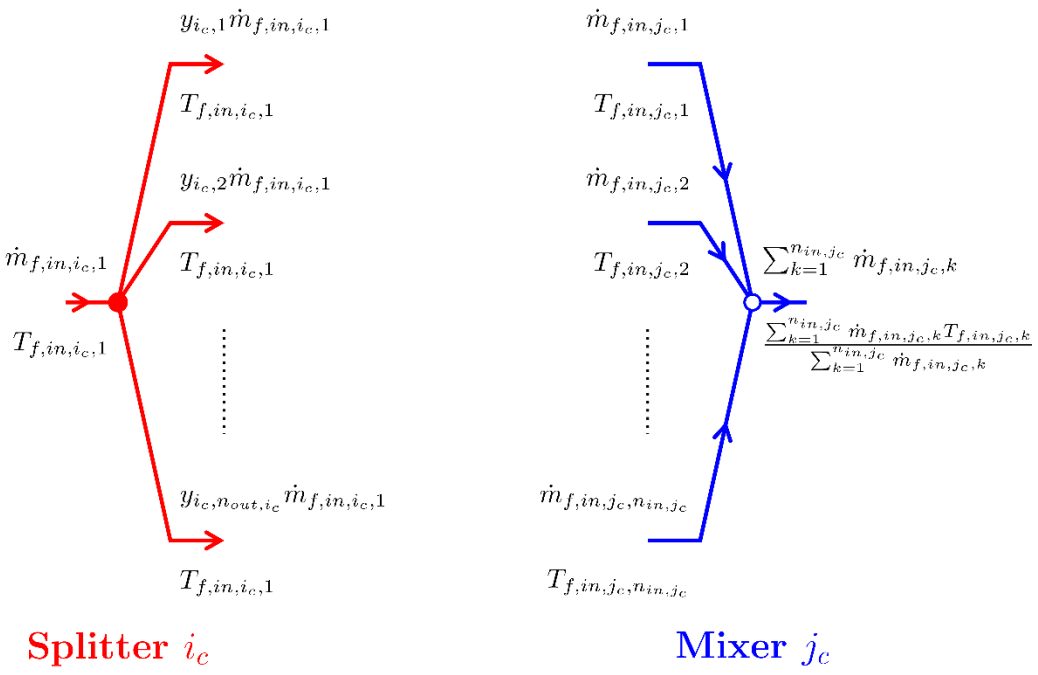

Figure 4. Fluid splitter and mixer system components

The flow mixer component mixes a given number n_{in,j_c} of fluid streams into a single fluid stream ($n_{out,j_c} = 1$), as shown on Figure 4. The outlet mass flow rate is the sum of the mass flow rates from all inlets. The outlet fluid temperature is the weighted sum of the inlet fluid temperatures by the inlet mass flow rates. The coefficient matrices and vectors for this component are given by:

$$\boldsymbol{a}_{\dot{\boldsymbol{m}}_{\boldsymbol{f,j_c}}} = \mathbf{1}_{1\times n_{in,j_c}} \tag{15}$$

$$\boldsymbol{b}_{\dot{\boldsymbol{m}}_{\boldsymbol{f,j_c}}} = 0 \tag{16}$$

$$\boldsymbol{a}_{\boldsymbol{T}_{\boldsymbol{f,j_c}}} = \boldsymbol{y}_{\boldsymbol{j_c}}^{\boldsymbol{T}} \tag{17}$$

$$\boldsymbol{b}_{\boldsymbol{T}_{\boldsymbol{f,j_c}}} = 0 \tag{18}$$

where $\boldsymbol{y_{j_c}} = \dot{\boldsymbol{m}}_{\boldsymbol{f,in,j_c}} \frac{1}{\mathbf{1}_{1\times n_{in,j_c}} \dot{\boldsymbol{m}}_{\boldsymbol{f,in,j_c}}}$ is a $n_{in,j_c} \times 1$ column vector of the inlet mass flow rate fractions relative to the outlet mass flow rate and is calculated after the inlet mass flow rates are solved.

2.1.3. Heat source

The heat source component, shown in Figure 5, serves as a heat source into a closed fluid loop and is also used to prescribe the mass flow rate in such loops. The relation between inlet and outlet fluid temperatures is obtained from an energy balance on the fluid with a known rate of heat transferred to the fluid. The coefficient matrices and vectors for this component are given by:

$$\boldsymbol{a}_{\dot{\boldsymbol{m}}_{\boldsymbol{f,i_c}}} = 0 \tag{19}$$

$$\boldsymbol{b}_{\dot{\boldsymbol{m}}_{\boldsymbol{f,i_c}}} = \dot{m}_{f,out,i_c,specified} \tag{20}$$

$$\boldsymbol{a}_{\boldsymbol{T}_{\boldsymbol{f,i_c}}} = 1 \tag{21}$$

$$\boldsymbol{b}_{\boldsymbol{T}_{\boldsymbol{f,i_c}}} = \frac{\dot{Q}_{i_c,specified}}{\dot{m}_{f,out,i_c,specified} c_p} \tag{22}$$

where $\dot{Q}_{i_c,specified}$ is the specified rate of heat transferred to the fluid.

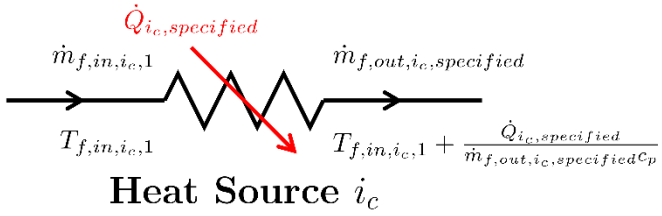

Figure 5. Heat source system component

2.1.4. Vertical borehole

A vertical geothermal borehole i_b is presented on Figure 6. The borehole has a radius r_{b,i_b}, a length H_{i_b} and is buried at a distance D_{i_b} from the ground surface. The borehole contains n_{p,i_b} U-tubes ($n_{p,i_b} = 2$ in Figure 6), for a total of $2n_{p,i_b}$ pipes. Each pipe i_p has an inner radius $r_{p,in}$, an outer radius $r_{p,out}$, and is placed at a position $\left(x_{i_p}, y_{i_p}\right)$ relative to the borehole axis. Fluid enters U-tube i_p at a temperature T_{f,in,i_b,i_p} and a mass flow rate $\dot{m}_{f,in,i_b,i_p}$ through pipe i_p and leaves through pipe $i_p + n_{p,i_b}$ at a temperature T_{f,out,i_b,i_p} and a mass flow rate $\dot{m}_{f,out,i_b,i_p} = \dot{m}_{f,in,i_b,i_p}$.

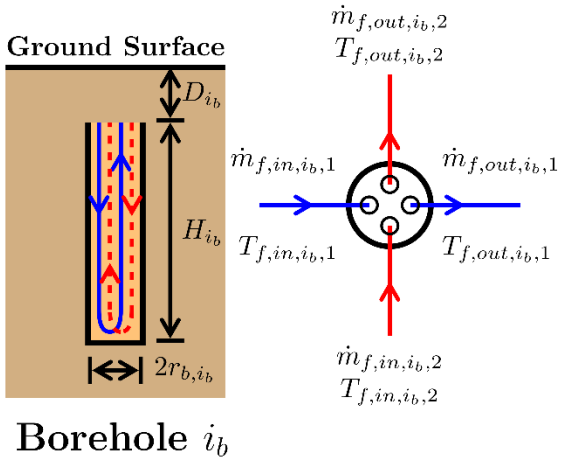

Figure 6. Vertical geothermal borehole with two independent U-tubes

The fluid temperature variations inside the borehole are driven by heat transfer between pipes and between individual pipes and the borehole wall. In the proposed methodology, the thermal capacity of the fluid and the borehole materials is neglected. Heat transfer inside the borehole is then treated as a steady-state process. Steady-state heat conduction inside a borehole cross section can be represented as a network of delta-circuit thermal resistances. From this delta-circuit, a system of differential equations is expressed for the axial variations of the fluid temperatures based on known borehole wall temperatures. Solving the system of differential

equations gives relations between inlet and outlet fluid temperatures and expressions for the heat extraction rates along the borehole. The derivation of the equations for heat transfer inside the borehole are presented in appendix from the analytical solutions of Cimmino (Cimmino 2016). Equation (A9) is repeated here:

$$\boldsymbol{E}_{\boldsymbol{out},\boldsymbol{i_b}}\left(H_{i_b}\right)\boldsymbol{T}_{\boldsymbol{f},\boldsymbol{out},\boldsymbol{i_b}} = \boldsymbol{E}_{\boldsymbol{in},\boldsymbol{i_b}}\left(H_{i_b}\right)\boldsymbol{T}_{\boldsymbol{f},\boldsymbol{in},\boldsymbol{i_b}} + \boldsymbol{E}_{\boldsymbol{b},\boldsymbol{i_b}}\left(H_{i_b}\right)\boldsymbol{T}_{\boldsymbol{b},\boldsymbol{i_b}} \tag{23}$$

where $\boldsymbol{E}_{\boldsymbol{out},\boldsymbol{i_b}}$ and $\boldsymbol{E}_{\boldsymbol{in},\boldsymbol{i_b}}$ are $n_{p,i_b} \times n_{p,i_b}$ coefficient matrices associated with the outlet and inlet fluid temperatures of borehole i_b, $\boldsymbol{E}_{\boldsymbol{b},\boldsymbol{i_b}}$ is a $n_{p,i_b} \times n_{q,i_b}$ coefficient matrix associated with borehole wall temperatures of borehole i_b and $\boldsymbol{T}_{\boldsymbol{b},\boldsymbol{i_b}}$ is a $n_{q,i_b} \times 1$ column vector of the borehole wall temperatures along the n_{q,i_b} segments of borehole i_b. The derivation of the coefficient matrices is presented in appendix. The division of boreholes into segments is necessary to consider the axial variations of the heat extraction rates along the boreholes. Values of borehole wall temperatures are obtained from the bore field heat transfer problem. The bore field heat transfer problem is later described in Section 2.3.

The coefficient matrix and vector for the heat balance problem of a borehole i_b corresponding to component i_c in the system are obtained by rearranging Equation (23). The coefficient matrices and vectors for a borehole component are given by:

$$\boldsymbol{a}_{\dot{\boldsymbol{m}}_{\boldsymbol{f},\boldsymbol{i_c}}} = \boldsymbol{I}_{n_{p,i_b}} \tag{24}$$

$$\boldsymbol{b}_{\dot{\boldsymbol{m}}_{\boldsymbol{f},\boldsymbol{i_c}}} = \boldsymbol{0}_{n_{p,i_b} \times n_{p,i_b}} \tag{25}$$

$$\boldsymbol{a}_{\boldsymbol{T}_{\boldsymbol{f},\boldsymbol{i_c}}} = \boldsymbol{E}^{-\boldsymbol{1}}_{\boldsymbol{out},\boldsymbol{i_b}}\left(H_{i_b}\right)\boldsymbol{E}_{\boldsymbol{in},\boldsymbol{i_b}}\left(H_{i_b}\right) \tag{26}$$

$$\boldsymbol{b}_{\boldsymbol{T}_{\boldsymbol{f},\boldsymbol{i_c}}} = \boldsymbol{E}^{-\boldsymbol{1}}_{\boldsymbol{out},\boldsymbol{i_b}}\left(H_{i_b}\right)\boldsymbol{E}_{\boldsymbol{b},\boldsymbol{i_b}}\left(H_{i_b}\right)\boldsymbol{T}_{\boldsymbol{b},\boldsymbol{i_b}} \tag{27}$$

where $\boldsymbol{I}_{n_{p,i_b}}$ is the $n_{p,i_b} \times n_{p,i_b}$ identity matrix. Note that the coefficient vector for the heat balance problem, $\boldsymbol{b}_{\boldsymbol{T}_{f,i_c}}$, is dependent on the borehole wall temperatures obtained from the bore field heat transfer problem.

2.2. System-level mass and heat balance problems

System-level mass and heat balance problems for the entire system may be constructed by assembly of the component-level mass and heat balance problems of each component in the system. The system-level problems have the same form as the component-level problems in Equations (1) and (2):

$$\dot{\boldsymbol{m}}_{\boldsymbol{f,out}} = \boldsymbol{A}_{\dot{\boldsymbol{m}}_{\boldsymbol{f}}} \dot{\boldsymbol{m}}_{\boldsymbol{f,in}} + \boldsymbol{B}_{\dot{\boldsymbol{m}}_{\boldsymbol{f}}} \tag{28}$$

$$\boldsymbol{T}_{\boldsymbol{f,out}} = \boldsymbol{A}_{\boldsymbol{T}_{\boldsymbol{f}}} \boldsymbol{T}_{\boldsymbol{f,in}} + \boldsymbol{B}_{\boldsymbol{T}_{\boldsymbol{f}}} \tag{29}$$

where $\boldsymbol{A}_{\dot{\boldsymbol{m}}_{\boldsymbol{f}}}$, $\boldsymbol{B}_{\dot{\boldsymbol{m}}_{\boldsymbol{f}}}$, $\boldsymbol{A}_{\boldsymbol{T}_{\boldsymbol{f}}}$ and $\boldsymbol{B}_{\boldsymbol{T}_{\boldsymbol{f}}}$ are system-level coefficient matrices and vectors for the mass and heat balance problems and are obtained by assembling the coefficient matrices and vectors from all components in the system:

$$\boldsymbol{A}_{\dot{\boldsymbol{m}}_{\boldsymbol{f}}} = \begin{bmatrix} \boldsymbol{a}_{\dot{\boldsymbol{m}}_{\boldsymbol{f},\mathbf{1}}} & \cdots & \mathbf{0} \\ \vdots & \ddots & \vdots \\ \mathbf{0} & \cdots & \boldsymbol{a}_{\dot{\boldsymbol{m}}_{\boldsymbol{f},\boldsymbol{N_c}}} \end{bmatrix}, \quad \boldsymbol{B}_{\dot{\boldsymbol{m}}_{\boldsymbol{f}}} = \begin{bmatrix} \boldsymbol{b}_{\dot{\boldsymbol{m}}_{\boldsymbol{f},\mathbf{1}}} \\ \vdots \\ \boldsymbol{b}_{\dot{\boldsymbol{m}}_{\boldsymbol{f},\boldsymbol{N_c}}} \end{bmatrix} \tag{30}$$

$$\boldsymbol{A}_{\boldsymbol{T}_{\boldsymbol{f}}} = \begin{bmatrix} \boldsymbol{a}_{\boldsymbol{T}_{\boldsymbol{f},\mathbf{1}}} & \cdots & \mathbf{0} \\ \vdots & \ddots & \vdots \\ \mathbf{0} & \cdots & \boldsymbol{a}_{\boldsymbol{T}_{\boldsymbol{f},\boldsymbol{N_c}}} \end{bmatrix}, \quad \boldsymbol{B}_{\mathrm{T}_{\boldsymbol{f}}} = \begin{bmatrix} \boldsymbol{b}_{\boldsymbol{T}_{\boldsymbol{f},\mathbf{1}}} \\ \vdots \\ \boldsymbol{b}_{\boldsymbol{T}_{\boldsymbol{f},\boldsymbol{N_c}}} \end{bmatrix} \tag{31}$$

$\dot{\boldsymbol{m}}_{\boldsymbol{f,in}}$, $\dot{\boldsymbol{m}}_{\boldsymbol{f,out}}$, $\boldsymbol{T}_{\boldsymbol{f,in}}$ and $\boldsymbol{T}_{\boldsymbol{f,out}}$ are system-level vectors of the inlet and outlet mass flow rates and fluid temperatures of all components in the system:

$$\dot{\boldsymbol{m}}_{\boldsymbol{f,in}} = \begin{bmatrix} \dot{\boldsymbol{m}}_{\boldsymbol{f,in,1}} \\ \vdots \\ \dot{\boldsymbol{m}}_{\boldsymbol{f,in,N_c}} \end{bmatrix}, \ \dot{\boldsymbol{m}}_{\boldsymbol{f,out}} = \begin{bmatrix} \dot{\boldsymbol{m}}_{\boldsymbol{f,out,1}} \\ \vdots \\ \dot{\boldsymbol{m}}_{\boldsymbol{f,out,N_c}} \end{bmatrix} \tag{32}$$

$$\boldsymbol{T}_{\boldsymbol{f,in}} = \begin{bmatrix} \boldsymbol{T}_{\boldsymbol{f,in,1}} \\ \vdots \\ \boldsymbol{T}_{\boldsymbol{f,in,N_c}} \end{bmatrix}, \ \boldsymbol{T}_{\boldsymbol{f,out}} = \begin{bmatrix} \boldsymbol{T}_{\boldsymbol{f,out,1}} \\ \vdots \\ \boldsymbol{T}_{\boldsymbol{f,out,N_c}} \end{bmatrix} \tag{33}$$

Equations (28) and (29) can't be solved at this stage, since both inlet and outlet values of the mass flow rates and fluid temperatures are unknown. To complete the formulation of the system-level problems, connections between outlets and inlets of system components need to be considered. Each outlet of each component is connected to an inlet of another component. As such, the relation between inlet and outlet mass flow rates and fluid temperatures are given by:

$$\dot{\boldsymbol{m}}_{\boldsymbol{f,in}} = \boldsymbol{C}\dot{\boldsymbol{m}}_{\boldsymbol{f,out}} \tag{34}$$

$$\boldsymbol{T}_{\boldsymbol{f,in}} = \boldsymbol{C}\boldsymbol{T}_{\boldsymbol{f,out}} \tag{35}$$

where $\boldsymbol{C}$ is the component connectivity matrix, structured as follows:

$$\boldsymbol{C} = \begin{bmatrix} c_{1,1} & \cdots & c_{1,N_{out}} \\ \vdots & \ddots & \vdots \\ c_{N_{in},1} & \cdots & c_{N_{in},N_{out}} \end{bmatrix} \tag{36}$$

For each outlet j_{out} of each component j_c connected to inlet i_{in} of component i_c, the matrix coefficient $c_{i,j} = 1$, where $i = i_{in} + \sum_{k=1}^{i_c-1} n_{in,k}$ and $j = j_{out} + \sum_{k=1}^{j_c-1} n_{out,k}$ are the cumulative indices of the connected outlet and inlet in the global system. All other matrix coefficients are zero.

Introducing Equations (34) and (35) into Equations (28) and (29), the system-level mass and heat balance problems can be solved for the outlet mass flow rates and fluid temperatures:

$$\dot{\boldsymbol{m}}_{\boldsymbol{f,out}} = \left(\boldsymbol{I}_{\boldsymbol{N_{out}}} - \boldsymbol{A}_{\dot{\boldsymbol{m}}_{\boldsymbol{f}}}\boldsymbol{C}\right)^{-\mathbf{1}} \boldsymbol{B}_{\dot{\boldsymbol{m}}_{\boldsymbol{f}}} \quad (37)$$

$$\boldsymbol{T}_{\boldsymbol{f,out}} = \left(\boldsymbol{I}_{\boldsymbol{N_{out}}} - \boldsymbol{A}_{\boldsymbol{T}_{\boldsymbol{f}}}\boldsymbol{C}\right)^{-\mathbf{1}} \boldsymbol{B}_{\boldsymbol{T}_{\boldsymbol{f}}} \quad (38)$$

where $N_{out} = \sum_{k=1}^{N_c} n_{out,k}$ is the total number of fluid outlets in the system and N_c is the number of system components.

The inlet mass flow rates and fluid temperatures can then be calculated from Equations (34) and (35).

2.3. Bore field heat transfer problem

2.3.1. Ground heat transfer

Ground temperature variations at the borehole walls due to extraction and injection of heat from and into the ground are calculated using the finite line source analytical solution (Cimmino and Bernier 2014). The ground is assumed to have uniform and isotropic thermal conductivity k_s and thermal diffusivity α_s, and the heat transfer process in the bore field is assumed to result only from conduction. The ground surface temperature is constant and equal to the undisturbed ground temperature $T_{g,0}$. Each borehole i_b is divided into a number n_{q,i_b} of borehole segments, each represented by a line heat source segment, as shown on Figure 7. The temperature drop at the wall of a segment u of a borehole i_b due to continuous heat extraction starting at time $t = 0$ at a segment v of a borehole j_b is given by:

$$\Delta T_{b,i_b,j_b,u,v}(t) = \frac{1}{2\pi k_s H_{i_b,u}} h_{i_b,j_b,u,v}(t)\dot{Q}_{b,j_b,v} \quad (39)$$

where $\Delta T_{b,i_b,j_b,u,v}$ is the temperature drop at the wall of a segment u of a borehole i_b due to

continuous heat extraction starting at time $t = 0$ at a segment v of a borehole j_b, $h_{i_b,j_b,u,v}$ is the segment-to-segment response factor from segment v of borehole j_b to segment u of borehole i_b and $\dot{Q}_{b,j_b,v}$ is the constant and uniform heat extraction rate over segment v of borehole j_b.

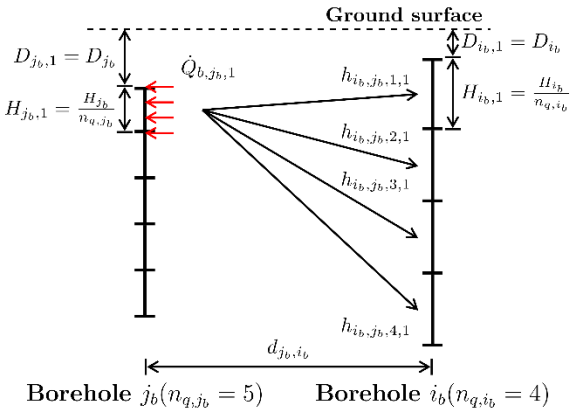

Figure 7. Segment-to-segment thermal response factors

The segment-to-segment response factors are given by the finite line source analytical solution (Cimmino and Bernier 2014):

$$h_{i_b,j_b,u,v}(t) = \frac{1}{2H_{i_b,u}} \int_{1/\sqrt{4\alpha_s t}}^{\infty} \frac{1}{s^2} \exp\left(-d_{i_b,j_b}^2 s^2\right) I_{FLS}(s) ds \tag{40}$$

$$I_{FLS}(s) = \text{erfint}\left(\left(D_{i_b,u} - D_{j_b,v} + H_{i_b,u}\right)s\right) - \text{erfint}\left(\left(D_{i_b,u} - D_{j_b,v}\right)s\right) + \text{erfint}\left(\left(D_{i_b,u} - D_{j_b,v} - H_{j_b,v}\right)s\right) - \text{erfint}\left(\left(D_{i_b,u} - D_{j_b,v} + H_{i_b,u} - H_{j_b,v}\right)s\right) + \text{erfint}\left(\left(D_{i_b,u} + D_{j_b,v} + H_{i_b,u}\right)s\right) - \text{erfint}\left(\left(D_{i_b,u} + D_{j_b,v}\right)s\right) + \text{erfint}\left(\left(D_{i_b,u} + D_{j_b,v} + H_{j_b,v}\right)s\right) - \text{erfint}\left(\left(D_{i_b,u} + D_{j_b,v} + H_{i_b,u} + H_{j_b,v}\right)s\right) \tag{41}$$

$$\text{erfint}(X) = \int_0^X \text{erf}(x')\, dx' = X\,\text{erf}(X) - \frac{1}{\sqrt{\pi}}\left(1 - \exp(-X^2)\right) \tag{42}$$

$$d_{i_b,j_b} = \begin{cases} r_{b,i_b} & \text{for } i = j \\ \sqrt{\left(x_{i_b} - x_{j_b}\right)^2 + \left(y_{i_b} - y_{j_b}\right)^2} & \text{for } i \neq j \end{cases} \quad (43)$$

where $H_{i_b,u} = H_{i_b}/n_{q,i_b}$ and $H_{j_b,v} = H_{j_b}/n_{q,j_b}$ are the lengths of segment u of borehole i_b and segment v of borehole j_b, respectively, $D_{i_b,u} = D_{i_b} + (u-1)\,H_{i_b}/n_{q,i_b}$ and $D_{j_b,v} = D_{j_b} + (v-1)\,H_{j_b}/n_{q,j_b}$ are the buried depths of segment u of borehole i_b and segment v of borehole j_b, respectively, and d_{i_b,j_b} is the radial distance between borehole i_b and borehole j_b, positioned at coordinates $\left(x_{i_b}, y_{i_b}\right)$ and $\left(x_{j_b}, y_{j_b}\right)$, respectively.

For a succession of heat extraction rates $\dot{Q}_{b,j_b,v}(t_k)$ constant over each time step $t_{k-1} < t \leq t_k$, with $\Delta t = t_k - t_{k-1}$ the simulation time step, the total borehole wall temperature variations are obtained from the spatial superposition of the finite line source solution of all line sources in the bore field:

$$\boldsymbol{T_b}(t_k) = \boldsymbol{T_{b,0}}(t_k) - \boldsymbol{H}(\Delta t)\dot{\boldsymbol{Q}}_{\boldsymbol{b}}(t_k) \quad (44)$$

where $\boldsymbol{T_b}$ is a $N_q \times 1$ column vector of the borehole wall temperatures at all segments of all boreholes, with $N_q = \sum_{i_b=1}^{N_b} n_{q,i_b}$ the total number of borehole segments in the bore field and N_b the number of boreholes, $\dot{\boldsymbol{Q}}_{\boldsymbol{b}}$ is a $N_q \times 1$ column vector of the heat extraction rates at all segments of all boreholes and $\boldsymbol{H}$ is a $N_q \times N_q$ matrix of the segment-to-segment thermal response factors. The borehole wall temperature and heat extraction rate vectors and the segment-to-segment response factor matrix are structured as follows:

$$\boldsymbol{T_b}(t_k) = \begin{bmatrix} \boldsymbol{T_{b,1}}(t_k) \\ \vdots \\ \boldsymbol{T_{b,N_b}}(t_k) \end{bmatrix}, \quad \boldsymbol{T_{b,i_b}}(t_k) = \begin{bmatrix} T_{b,i_b,1}(t_k) \\ \vdots \\ T_{b,i_b,n_{q,i_b}}(t_k) \end{bmatrix} \quad (45)$$

$$\dot{\boldsymbol{Q}}_{\boldsymbol{b}}(t_k) = \begin{bmatrix} \dot{\boldsymbol{Q}}_{\boldsymbol{b,1}}(t_k) \\ \vdots \\ \dot{\boldsymbol{Q}}_{\boldsymbol{b},\boldsymbol{N_b}}(t_k) \end{bmatrix}, \quad \dot{\boldsymbol{Q}}_{\boldsymbol{b},\boldsymbol{i_b}}(t_k) = \begin{bmatrix} \dot{Q}_{b,i_b,1}(t_k) \\ \vdots \\ \dot{Q}_{b,i_b,n_{q,i_b}}(t_k) \end{bmatrix} \tag{46}$$

$$\boldsymbol{H}(t) = \begin{bmatrix} \boldsymbol{H_{1,1}}(t) & \cdots & \boldsymbol{H_{1,N_b}}(t) \\ \vdots & \ddots & \vdots \\ \boldsymbol{H_{N_b,1}}(t) & \cdots & \boldsymbol{H_{N_b,N_b}}(t) \end{bmatrix}, \quad \boldsymbol{H_{i_b,j_b}}(t) =$$

$$\frac{1}{2\pi k_s H_{i_b}/n_{q,i_b}} \begin{bmatrix} h_{i_b,j_b,1,1}(t) & \cdots & h_{i_b,j_b,1,n_{q,j_b}}(t) \\ \vdots & \ddots & \vdots \\ h_{i_b,j_b,n_{q,i_b},1}(t) & \cdots & h_{i_b,j_b,n_{q,i_b},n_{q,j_b}}(t) \end{bmatrix} \tag{47}$$

$\boldsymbol{T_{b,0}}(t_k)$ in Equation (44) is a $N_q \times 1$ column vector of the borehole wall temperatures at all segments of all boreholes assuming no heat extraction at any borehole segment over $t_{k-1} < t \leq t_k$. This temperature vector is obtained from the temporal and spatial superpositions of the finite line source solution for all time steps preceding time t_k:

$$\boldsymbol{T_{b,0}}(t_k) = \boldsymbol{T_g}(t_k) - \sum_{p=1}^{k-1} \left(\boldsymbol{H}(t_k - t_{p-1}) - \boldsymbol{H}(t_k - t_p) \right) \dot{\boldsymbol{Q}}_{\boldsymbol{b}}(t_p) \tag{48}$$

where $\boldsymbol{T_g}$ is a $N_q \times 1$ column vector of the undisturbed ground temperatures at all segments of all boreholes.

The summation process in Equation (48) becomes increasingly expensive in terms of computational time as the number of time steps in the simulation increases. Additionally, Equation (48) requires the evaluation of the segment-to-segment thermal response factors at all times t_k of the simulation, which in the case of the finite line source solution (Equation (40)) requires numerical evaluations of an integral. To accelerate the temporal superposition process, the load aggregation method of Claesson and Javed (Claesson and Javed 2012) is employed. This load aggregation method averages past heat extraction rates into a limited number of so-called

load aggregation cells. The size of load aggregation cells doubles at each level of aggregation. Six cells per level of aggregation are used in this work. The size of a given load aggregation cell is given by:

$$\Delta t_p = 2^{v-1}\Delta t \tag{49}$$

$$v = \text{ceil}\left({}^{p}/_{6}\right) \tag{50}$$

where Δt_p is the size of load aggregation cell p.

Aggregated loads are shifted one time step every time step of the simulation:

$$\overline{\boldsymbol{Q}}_{\boldsymbol{b,p}}^{(\boldsymbol{k})} = \begin{cases} \overline{\boldsymbol{Q}}_{\boldsymbol{b,j,p-1}}^{(\boldsymbol{k-1})} \frac{\Delta t}{\Delta t_p} + \overline{\boldsymbol{Q}}_{\boldsymbol{b,j,p}}^{(\boldsymbol{k-1})} \frac{\Delta t_p - \Delta t}{\Delta t_p}, & t_p^* < t_k \\ \overline{\boldsymbol{Q}}_{\boldsymbol{b,j,p-1}}^{(\boldsymbol{k-1})} \frac{\Delta t}{\Delta t_p} + \overline{\boldsymbol{Q}}_{\boldsymbol{b,j,p}}^{(\boldsymbol{k-1})}, & t_p^* \geq t_k \text{ and } t_{p-1}^* < t_k \\ 0, & t_{p-1}^* \geq t_k \end{cases} \tag{51}$$

where $\overline{\boldsymbol{Q}}_{\boldsymbol{b,1}}^{(\boldsymbol{k})} = \dot{\boldsymbol{Q}}_{\boldsymbol{b}}(t_k)$ is the value of the aggregated heat extraction rates in the first aggregation cell at the k-th time step, equal to the value of the heat extraction rates at time t_k.

The result of the temporal superposition of Equation (48) is estimated based on the aggregated values of the heat extraction rates:

$$\boldsymbol{T}_{\boldsymbol{b,0}}(t_k) = \boldsymbol{T}_{\boldsymbol{g}}(t_k) - \sum_{p=2}^{N_{agg}} \left(\boldsymbol{H}\left(t_p^*\right) - \boldsymbol{H}\left(t_{p-1}^*\right)\right) \overline{\boldsymbol{Q}}_{\boldsymbol{b,p}}^{(\boldsymbol{k})} \tag{52}$$

where $t_p^* = \sum_{k=1}^{p} \Delta t_p$ is the time associated with load aggregation cell p and N_{agg} is the total number of load aggregation cells. In addition to decreasing the number of terms in the temporal superposition process, Equation (52) only requires the evaluation of the segment-to-segment response factors at a limited number N_{agg} of time values t_p^*.

2.3.2. Borehole heat transfer

When the heat extraction rates are known, the borehole wall temperatures may be simply calculated from the combination of Equations (44) and (52). However, in the present case, the fluid network model returns the inlet fluid temperatures into the boreholes. For any borehole i_b, a linear relation between borehole wall temperatures and borehole heat extraction rates is assumed:

$$\dot{\boldsymbol{Q}}_{\boldsymbol{b},\boldsymbol{i_b}}(t_k) = \boldsymbol{a}_{\boldsymbol{Q}_{\boldsymbol{b},\boldsymbol{i_b}}} \boldsymbol{T}_{\boldsymbol{b},\boldsymbol{i_b}}(t_k) + \boldsymbol{b}_{\boldsymbol{Q}_{\boldsymbol{b},\boldsymbol{i_b}}} \tag{53}$$

where $\boldsymbol{a}_{\boldsymbol{Q}_{\boldsymbol{b},\boldsymbol{i_b}}}$ is a $n_{q,i_b} \times n_{q,i_b}$ matrix of coefficients and $\boldsymbol{b}_{\boldsymbol{Q}_{\boldsymbol{b},\boldsymbol{i_b}}}$ is a $n_{q,i_b} \times 1$ column vector of coefficients for the heat transfer problem in borehole i_b.

As shown in the borehole heat transfer model presented in appendix, the borehole heat extraction rates of a borehole i_b are obtained from its borehole wall temperatures and inlet fluid temperatures. Equation (A16) for borehole heat extraction rates is repeated here:

$$\dot{\boldsymbol{Q}}_{\boldsymbol{b},\boldsymbol{i_b}}(t_k) = -\boldsymbol{\Delta F}_{\boldsymbol{i_b}} \boldsymbol{T}_{\boldsymbol{b},\boldsymbol{i_b}}(t_k) + \boldsymbol{\Delta E}_{\boldsymbol{i_b}} \begin{bmatrix} \boldsymbol{I}_{n_{p,i_b}} \\ \boldsymbol{E}^{-\boldsymbol{1}}_{\boldsymbol{out},\boldsymbol{i_b}}(H_{i_b}) \boldsymbol{E}_{\boldsymbol{in},\boldsymbol{i_b}}(H_{i_b}) \end{bmatrix} \boldsymbol{T}_{\boldsymbol{f},\boldsymbol{in},\boldsymbol{i_b}} \tag{54}$$

where $\boldsymbol{\Delta F}_{\boldsymbol{i_b}}$ is a $n_{q,i_b} \times n_{q,i_b}$ coefficient matrix and $\boldsymbol{\Delta E}_{\boldsymbol{i_b}}$ is a $n_{q,i_b} \times n_{p,i_b}$ coefficient matrix. The derivation of the coefficient matrices is presented in appendix.

As mentioned in Section 2.1, while a steady-state analytical model of the borehole heat transfer is used in the present work, any suitable model could be used in the proposed methodology, given that the relationships between inlet and outlet fluid temperatures and between borehole wall temperatures and borehole heat extraction rates are expressed in the form of Equations (2) and (53). Non-linear terms may be included into the coefficient vectors $\boldsymbol{b}_{\boldsymbol{T}_{\boldsymbol{f},\boldsymbol{ic}}}$ and $\boldsymbol{b}_{\boldsymbol{Q}_{\boldsymbol{b},\boldsymbol{i_b}}}$, if necessary.

From Equation (54), the matrix and vector of coefficients for the borehole heat transfer problem are given by:

$$\boldsymbol{a}_{\boldsymbol{Q}_{b,i_b}} = -\boldsymbol{\Delta F}_{\boldsymbol{i_b}} \tag{55}$$

$$\boldsymbol{b}_{\boldsymbol{Q}_{b,i_b}} = \boldsymbol{\Delta E}_{\boldsymbol{i_b}} \begin{bmatrix} \boldsymbol{I}_{n_{p,i_b}} \\ \boldsymbol{E}_{\boldsymbol{out},\boldsymbol{i_b}}^{-\boldsymbol{1}}(H_{i_b})\boldsymbol{E}_{\boldsymbol{in},\boldsymbol{i_b}}(H_{i_b}) \end{bmatrix} \boldsymbol{T}_{\boldsymbol{f},\boldsymbol{in},\boldsymbol{i_b}} \tag{56}$$

The borehole heat transfer problem is formulated for all boreholes in the bore field. As was done for the mass and heat balance problems of the component models, a global system of equations can be assembled from the individual borehole heat transfer problems. The global bore field heat transfer problem and the global coefficient matrices and vector are given by:

$$\dot{\boldsymbol{Q}}_{\boldsymbol{b}} = \boldsymbol{A}_{\boldsymbol{Q}_b}\boldsymbol{T}_{\boldsymbol{b}} + \boldsymbol{B}_{\boldsymbol{Q}_b} \tag{57}$$

$$\boldsymbol{A}_{\boldsymbol{Q}_b} = \begin{bmatrix} \boldsymbol{a}_{\boldsymbol{Q}_{b,1}} & \cdots & \boldsymbol{0} \\ \vdots & \ddots & \vdots \\ \boldsymbol{0} & \cdots & \boldsymbol{a}_{\boldsymbol{Q}_{b,N_b}} \end{bmatrix}, \quad \boldsymbol{B}_{\boldsymbol{Q}_b} = \begin{bmatrix} \boldsymbol{b}_{\boldsymbol{Q}_{b,1}} \\ \vdots \\ \boldsymbol{b}_{\boldsymbol{Q}_{b,N_b}} \end{bmatrix} \tag{58}$$

Introducing Equation (57) into Equation (44), the borehole wall temperatures can be calculated for the given inlet fluid temperatures:

$$\boldsymbol{T}_{\boldsymbol{b}}(t_k) = \left(\boldsymbol{I}_{N_q} + \boldsymbol{H}(\Delta t)\boldsymbol{A}_{\boldsymbol{Q}_b}\right)^{-\boldsymbol{1}} \left(\boldsymbol{T}_{\boldsymbol{b},\boldsymbol{0}}(t_k) - \boldsymbol{H}(\Delta t)\boldsymbol{B}_{\boldsymbol{Q}_b}\right) \tag{59}$$

Following the calculation of borehole wall temperatures, heat extraction rates can be calculated from Equation (57) when required for the aggregation of loads (Equations (51) and (52)). The formulation presented in Equation (59) greatly reduces the size of the system of equations to be solved when compared to other formulations where both the borehole wall

temperatures and heat extraction rates are evaluated simultaneously, as for example in (Cimmino 2016). The inverted matrix $\left(\boldsymbol{I}_{N_q} + \boldsymbol{H}(\Delta t)\boldsymbol{A}_{\boldsymbol{Q}_b}\right)$ is then only of size $N_q \times N_q$, rather than $\left(2N_q + 2N_p\right) \times \left(2N_q + 2N_p\right)$, where $N_p = \sum_{i_b=1}^{N_b} n_{p,i_b}$ is the total number of U-tubes in the bore field.

2.4. Numerical solution method

The inlet and outlet fluid mass flow rates and temperatures in the system and the borehole wall temperatures in the bore field are evaluated by solving Equations (37), (38) and (59). Since the coefficients matrices and vectors in any of these equations may be dependent on the results of the other two equations, an iterative procedure is required. The numerical solution algorithm is presented on Figure 8. Fluid mass flow rates are solved at a relative tolerance $\varepsilon_{rel,\dot{m}_f} \geq \max_{i_c,m}\left|\frac{\dot{m}_{f,out,i_c,m}^{(n)} - \dot{m}_{f,out,i_c,m}^{(n-1)}}{\dot{m}_{f,out,i_c,m}^{(n-1)}}\right|$, where $\dot{m}_{f,in,i_c,m}^{(n)}$ is the inlet mass flow rate at inlet m of component i_c evaluated at iteration n. The inlet fluid temperatures and borehole wall temperatures are evaluated at absolute tolerances $\varepsilon_{abs,T_f} \geq \max_{i_c,m}\left|T_{f,out,i_c,m}^{(n)} - T_{f,out,i_c,m}^{(n-1)}\right|$ and $\varepsilon_{abs,T_b} \geq \max_{i_b,u}\left|T_{b,i_b,u}^{(n)} - T_{b,i_b,u}^{(n-1)}\right|$.

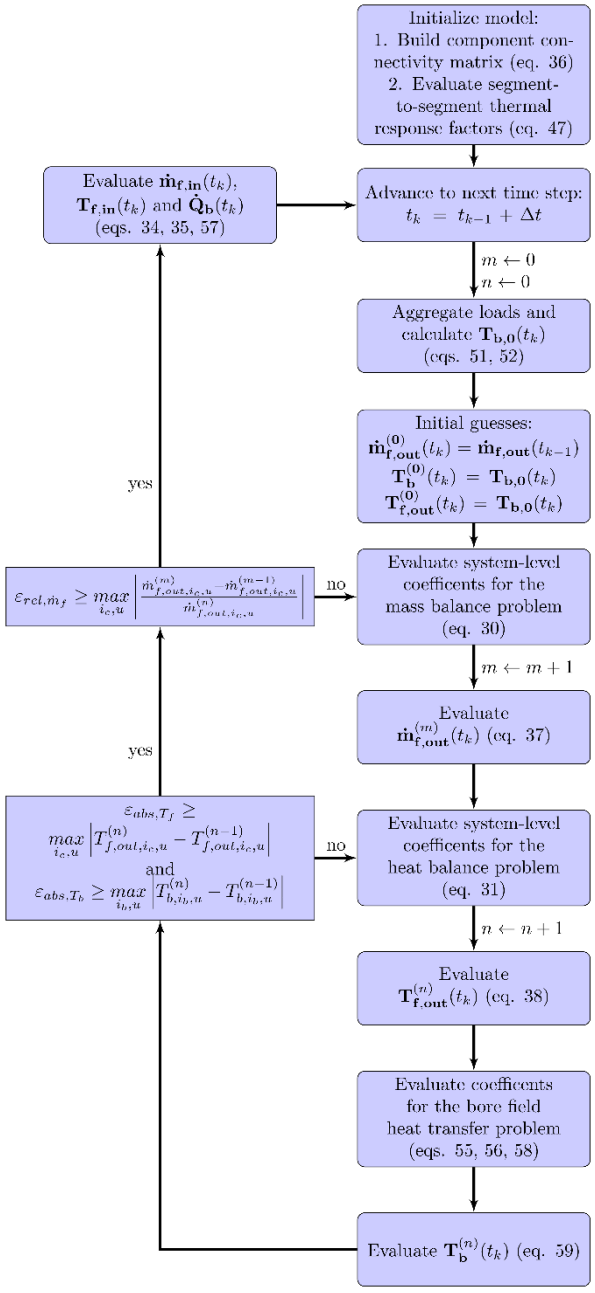

Figure 8. Numerical solution algorithm

The numerical solution algorithm presented in Figure 8 has two iterative loops: one for mass flow rates (the outer loop) and one for fluid and borehole wall temperatures (the inner loop). The inner iterative loop is always required because coefficients for the heat balance problem in the boreholes and for the bore field heat transfer problem are dependent on both fluid

and borehole wall temperatures. However, the matrix inverses in the system-level heat and mass balance problems and in the bore field heat transfer problem (Equations (37), (38) and (59)) can be stored and updated only when matrix coefficients (i.e. $\boldsymbol{a}_{\dot{m}_{f,i_c}}$, $\boldsymbol{a}_{T_{f,i_c}}$ and $\boldsymbol{a}_{Q_{b,i_b}}$) are modified. For the system components presented in this paper, these matrix coefficients only sometimes change when the mass flow rates change. The outer loop can be omitted in cases where the mass flow rates are not dependent on fluid temperatures.

3. Results

The capabilities of the simulation model are tested in 20 year hourly simulations of 3 different geothermal heat pump systems for a 5,000 sq-ft office building located in Montreal, Canada. The building heating and cooling loads are evaluated in eQuest 3.65. The peak heating load is 80.7 kW and the total required heating energy is 37,715 kWh. The peak cooling load is 46.4 kW and the total required cooling energy is 12,907 kWh. The hourly building heating (positive) and cooling (negative) loads are shown in Figure 9a. Simulation parameters shared by the 3 systems are presented in table 1. In all cases, simulations were done using absolute tolerances on temperatures $\varepsilon_{abs,T_f} = \varepsilon_{abs,T_b} = 0.001$°C and a relative tolerance on fluid mass flow rates $\varepsilon_{rel,\dot{m}_f} = 1\times10^{-6}$. All calculations were executed on the same computer equipped with a 4.2 GHz quad core (8 threads) processor. The simulation model was implemented in Python 2.7.

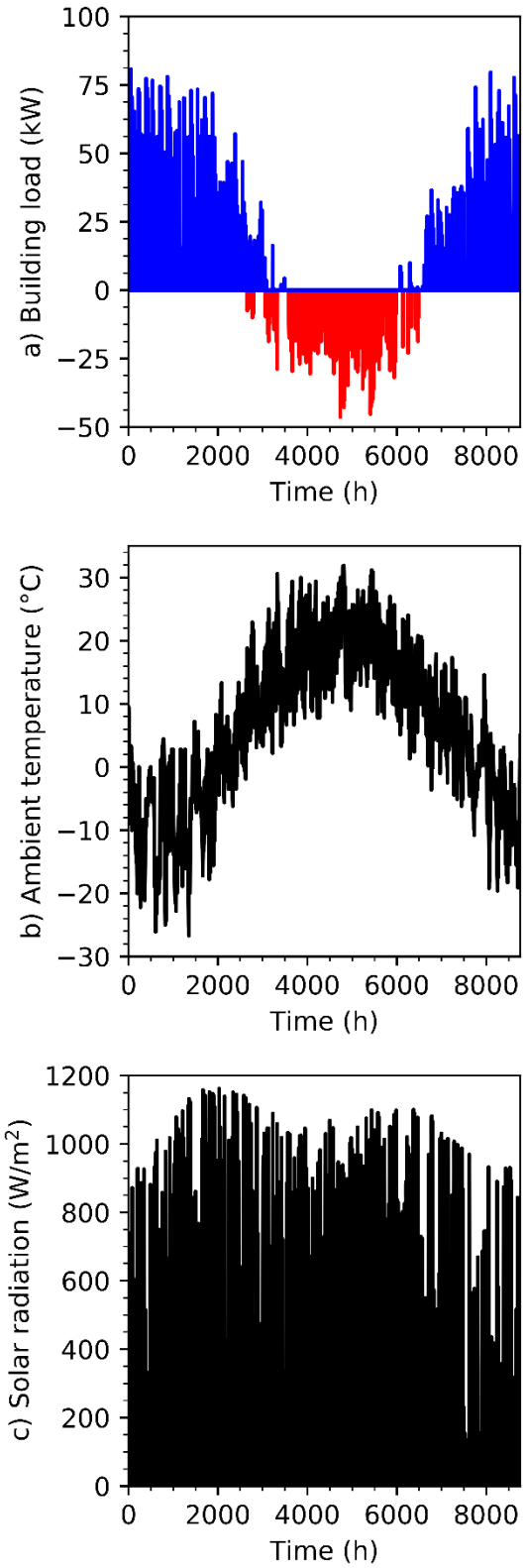

Figure 9. (a) Building loads, (b) ambient temperatures, and (c) solar radiation on solar collectors

Table 1. Simulation parameters

Parameter	Value	
Simulation time step	1	h
Maximum time	20	years
Number of segments (per borehole)	12	(-)
Buried depth	2.5	m
Borehole length	variable	m
Borehole spacing	5	m
Borehole radius	0.075	m
Pipe outer radius	0.017	m
Pipe inner radius	0.013	m
Shank spacing (center-to-center)	0.040	m
Undisturbed ground temperature	10	°C
Ground thermal conductivity	2.5	W/m-K
Ground thermal diffusivity	1×10^{-6}	m^2/s
Grout thermal conductivity	1.0	W/m-K
Pipe thermal conductivity	0.4	W/m-K
Fluid thermal conductivity	0.47	W/m-K
Fluid dynamic viscosity	2.79×10^{-3}	Pa-s
Fluid density	1024	kg/m^3
Fluid specific heat	3951	J/kg-K

A ground-source heat pump provides both heating and cooling to the building. It is assumed that the heat pump capacity is sufficient to cover the peak heating and cooling loads. The heat pump coefficient of performance (COP) in the two modes are given by:

$$COP = \begin{cases} 3.896 \cdot 10^{-4} T_{f,in,i_c}^2 + 6.170 \cdot 10^{-2} T_{f,in,i_c} + 3.376 & \text{if } \dot{Q}_{building} \leq 0 \text{ (Heating)} \\ 5.478 \cdot 10^{-5} T_{f,in,i_c}^2 - 1.206 \cdot 10^{-1} T_{f,in,i_c} + 8.431 & \text{if } \dot{Q}_{building} > 0 \text{ (Cooling)} \end{cases} \quad (60)$$

where $T_{f,in,i}$ is the inlet fluid temperature into the heat source component representing the heat pump. The specified heat transfer rate of the heat source representing the heat pump is then:

$$\dot{Q}_{i_c,specified} = \begin{cases} \dot{Q}_{building}\left(1 - \frac{1}{COP}\right) & \text{if } \dot{Q}_{building} \leq 0 \text{ (Heating)} \\ \dot{Q}_{building}\left(1 + \frac{1}{COP}\right) & \text{if } \dot{Q}_{building} > 0 \text{ (Cooling)} \end{cases} \quad (61)$$

In the second and third presented cases, flat plate solar collectors are used to store solar thermal energy in the bore field and raise ground temperatures. The solar collectors have an

effective area of 2.2 m^2, a slope $\beta = 45°$ and face true south ($\gamma = 0°$). The solar collector efficiency is given by:

$$\eta = 0.80 - 3.71\frac{\bar{T}_f - T_a}{G} - 0.01\frac{(\bar{T}_f - T_a)^2}{G} \quad (62)$$

where η is the solar collector efficiency, $\bar{T}_f = 0.5\left(T_{f,in,j_c} + T_{f,out,j_c}\right)$ is the mean temperature in the solar collectors, T_a is the ambient temperature and G is the captured solar radiation. Hourly ambient temperatures are shown on Figure 9b and captured solar radiation by the tilted solar collectors on Figure 9c. The specified heat transfer rate of the heat source representing the solar collectors is then:

$$\dot{Q}_{j_c,specified} = \max(G\eta, 0) \quad (63)$$

3.1. Field of 16 parallel-connected boreholes

A field of 16 boreholes positioned in a 4 × 4 array and connected in parallel is shown on Figure 10. The system includes a total of 19 components: 16 boreholes (1-16), a heat source (17), a flow splitter (18) and a flow mixer (19). Note that the piping pattern on Figure 10 is meant to represent the connections between the components as seen by the system model and not the actual piping pattern as would be seen in practice, although the two might be equivalent. Boreholes are equally spaced on a 4 × 4 rectangular grid with a spacing $B = 5$ m. The borehole length $H = 115$ m is equal for all boreholes and was chosen to obtain a minimum fluid temperature of 0°C in the system during the 20th simulation year and rounded up to the nearest 5 m increment. The nominal fluid mass flow rate into the bore field is 4 kg/s and is evenly distributed amongst the boreholes. At all times when the heat pump is turned off ($\dot{Q}_{i_c,specified} =$

0), the mass flow rate is reduced to 5% of its nominal value. This is to approach the condition of no flow in the boreholes and avoid numerical errors associated with zero flow in the borehole heat transfer model.

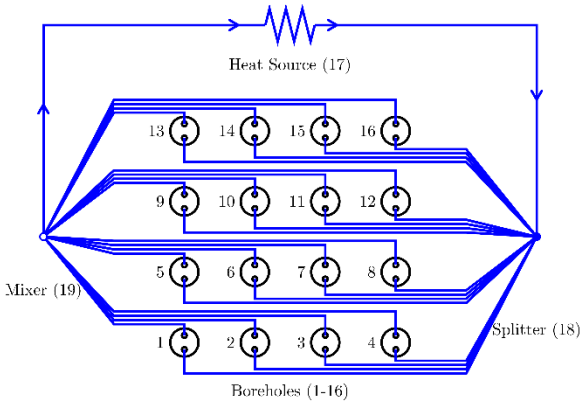

Figure 10. Field of 16 parallel-connected boreholes

Simulation results are verified against a simulation using the corresponding g-function for the bore field presented in Figure 10. The g-function is calculated using the finite line source method of Cimmino (Cimmino 2015), which assumes the inlet temperature into the boreholes are equal and accounts for the thermal interaction between U-tube pipes and between each U-tube pipe and the borehole wall. The simulation using the g-function method uses the total heat extraction rate calculated from the simulation using the presented methodology. The average borehole wall temperature in the bore field and the inlet and outlet fluid temperatures are then given by:

$$\bar{T}_b(t_k) = \bar{T}_{b,0}(t_k) - \frac{g(\Delta t)}{2\pi k_s H_{tot}} \dot{Q}_{tot}(t_k) \qquad (64)$$

$$\bar{T}_f(t_k) = \bar{T}_b(t_k) - \frac{\dot{Q}_{tot}(t_k)}{H_{tot}} R_b^* \qquad (65)$$

$$T_{f,in}(t_k) = \bar{T}_f(t_k) - 0.5 \frac{\dot{Q}_{tot}(t_k)}{\dot{m}_{f,in} c_p} \qquad (66)$$

$$T_{f,out}(t_k) = \bar{T}_f(t_k) + 0.5\frac{\dot{Q}_{tot}(t_k)}{\dot{m}_{f,in}c_p} \qquad (67)$$

where $\bar{T}_b$ is the average borehole wall temperature in the bore field, $\bar{T}_{b,0}$ is the average borehole wall temperature assuming no heat extraction during the current time step calculated using a temporal superposition procedure equivalent to Equation (52), $\bar{T}_f$ is the arithmetic average of the inlet and outlet fluid temperatures, $\dot{Q}_{tot} = -\dot{Q}_{i_c,specified}$ is the total heat extraction rate in the bore field, $H_{tot} = N_b H$ is the total borehole length, $R_b^* = 0.177$ m-K/W is the effective borehole thermal resistance and g is the g-function.

Calculated average borehole wall temperatures and inlet and outlet fluid temperatures and the total heat extraction rate using the proposed method and using the g-function method are presented in Figure 11 for hours 697-816 (5 weekdays, starting January 30th) of the 20th simulation year. It is shown that the predicted fluid and borehole wall temperatures are in close agreement: the maximum absolute difference (over all 20 years) on predicted temperatures is 0.019°C. During the 20th simulation year, the minimum fluid temperature is 0.12°C, the total heat extracted is 27,663 kWh and the total heat injected is 14,753 kWh.

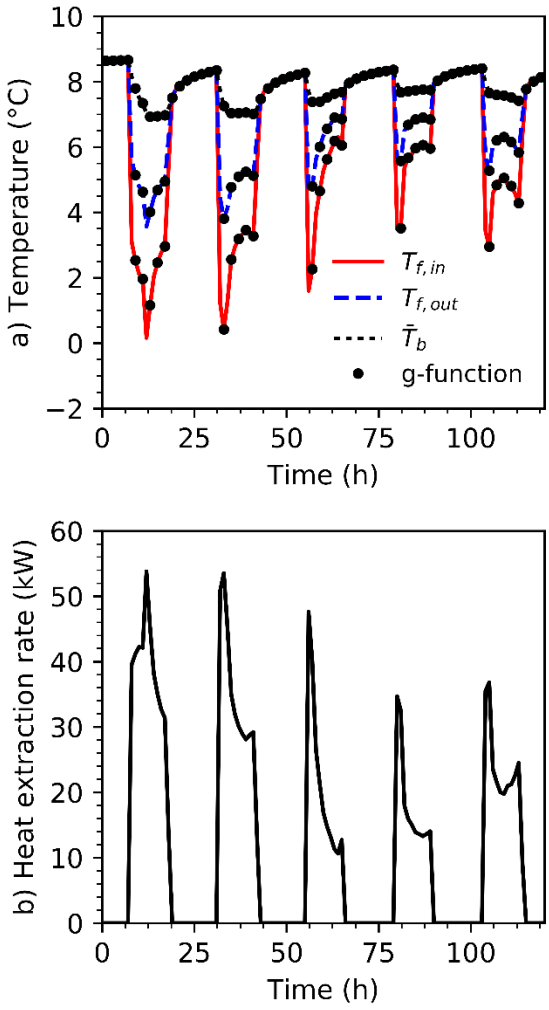

Figure 11. (a) Temperatures and (b) total heat extraction rates during five days of the 20th simulation year of the field of 16 parallel-connected boreholes

The total simulation time using the presented methodology is 5,040 seconds, where 15 seconds is the computational time required for the initialization of the component models including the calculation of the segment-to-segment response factors, 2,766 seconds is the computational time required for the temporal superposition algorithm and 2,186 seconds is the computational time required for the solution of the coupled system-level heat and mass balance problems and the bore field heat transfer problem. Note that the simulation time is heavily dependent on the number of segments used to discretize the boreholes: the simulation time using

1 segment per borehole (16 segments in total), rather than 12 segments per borehole (192 segments in total), is 457 seconds with 171 seconds spent on temporal superposition.

3.2. Field of 16 parallel-connected boreholes with independent network of 8 parallel-connected boreholes

In this second case, 8 boreholes are added to the previous bore field and independently connected to an array of 16 flat plate solar collectors (35 m^2 total effective area). The borehole positions are shown in Figure 12a and the system configuration for the added boreholes and solar collectors is shown on Figure 12b. The system includes a total of 30 components: 16 boreholes (1-16) connected to the heat pump, 8 boreholes (17-24) connected to the solar collectors, a heat source (25) representing the heat pump, a heat source (26) representing the solar collectors, two flow splitters (27-28) and two flow mixers (29-30). The borehole length is $H_1 = 85$ m for boreholes connected to the heat pump and $H_2 = H_1/3$ for boreholes connected to the solar collectors. Solar heat is stored in the second circuit to eventually raise the bore field temperature and allow for a reduced borehole length of the boreholes in the first circuit. The nominal fluid mass flow rate into the independent network of boreholes is 0.7 kg/s and is evenly distributed among the boreholes. As in the previous case, at all times when the solar collectors are not providing heat ($\dot{Q}_{j_c,specified} = 0$), the mass flow rate is reduced to 5% of its nominal value.

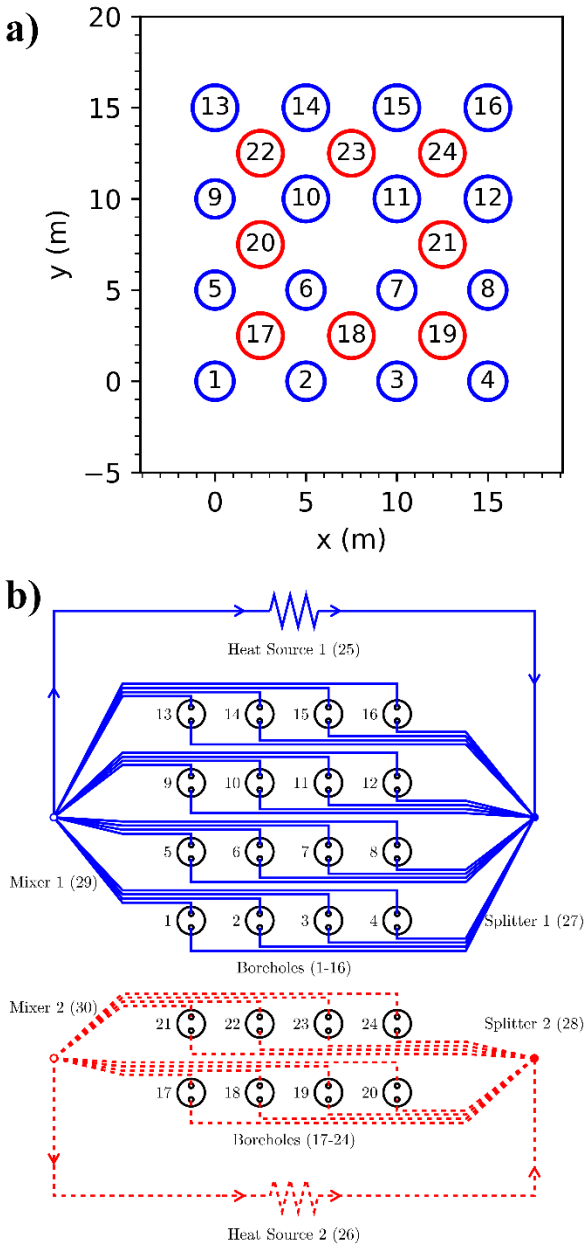

Figure 12. Field of 16 parallel-connected boreholes with independent cluster of 8 parallel-connected boreholes: (a) borehole positions, and (b) system configuration

Calculated average borehole wall temperatures and inlet and outlet fluid temperatures and the total heat extraction rate using the proposed method are presented in Figure 13 for hours 697-816 (5 weekdays, starting January 30th) of the 20th simulation year. During the 20th simulation year, the minimum fluid temperature is 0.47°C, the total heat extracted by the heat pump is

27,913 kWh, the total heat injected by the heat pump is 14,895 kWh and the total heat injected by the solar collectors is 34,098 kWh. The borehole wall and fluid temperature profiles of boreholes 5 and 20 are shown on Figure 14 for hour 756 of the last year (February 1st at 12:00pm). It is shown that the boreholes connected to the solar collectors have successfully raised the ground temperature in the bore field: at this time, the borehole wall temperature of the upper third of borehole 5 is 1.09°C greater than the rest of its length.

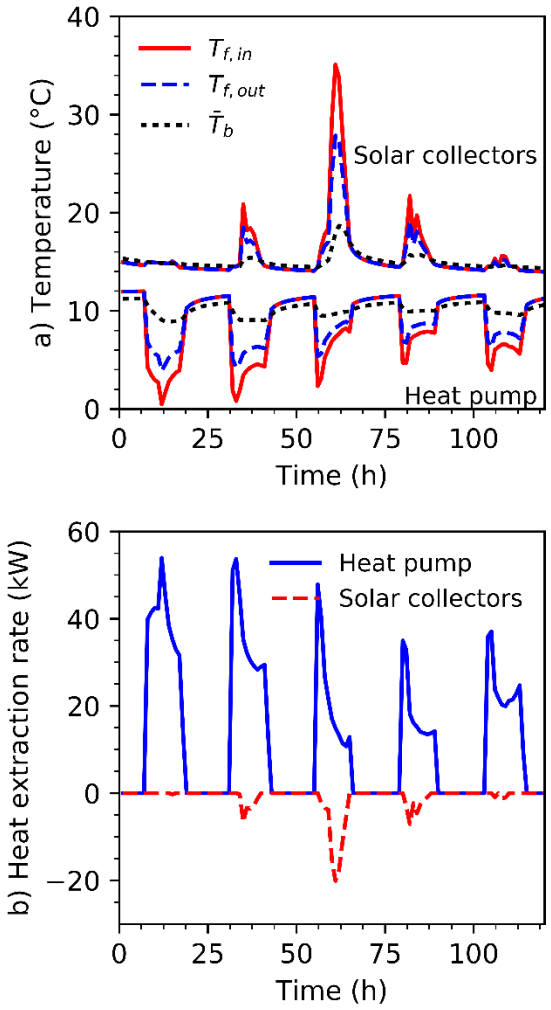

Figure 13. (a) Temperatures and (b) total heat extraction rates during five days of the 20th simulation year of the field of 16 parallel-connected boreholes with independent cluster of 8 parallel-connected boreholes

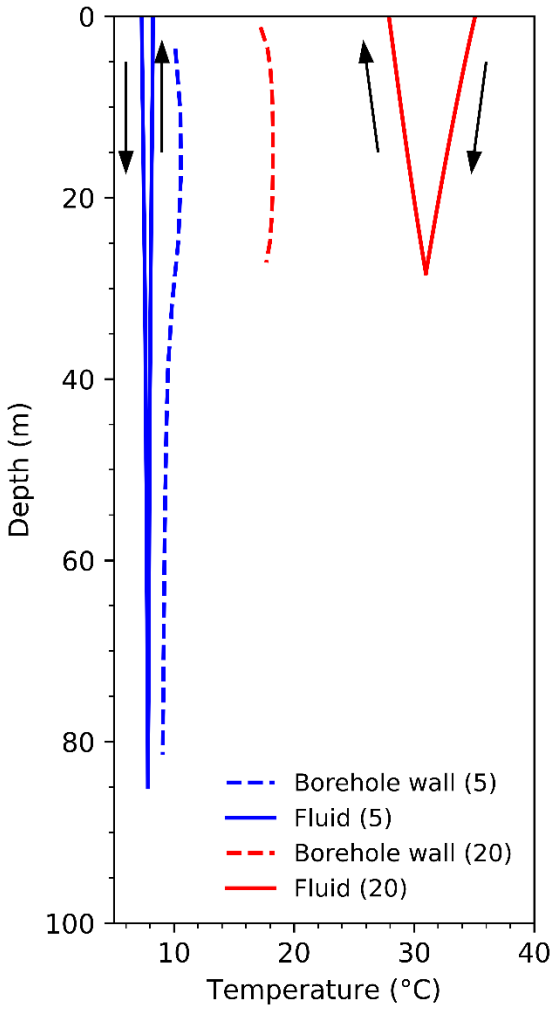

Figure 14. Fluid and borehole wall temperature profiles of boreholes 5 and 20

The total simulation time using the presented methodology is 14,257 seconds, where 41 seconds is the computational time required for the initialization of the component models including the calculation of the segment-to-segment response factors, 10,263 seconds is the computational time required for the temporal superposition algorithm and 3,847 seconds is the computational time required for the solution of the coupled system-level heat and mass balance problems and the bore field heat transfer problem.

3.3. Field of 16 boreholes in 4 parallel branches of 4 series-connected boreholes with two independent circuits in counterflow

In this third case, 16 boreholes are divided into 4 parallel branches of 4 boreholes each. Each borehole has two independent U-tubes connected in series with other boreholes of the same branch. Boreholes are positioned on concentric involute spirals with an even spacing B = 5 m between two adjacent branches and between two boreholes of the same branch. The borehole positions are shown in Figure 15 and the system configuration was previously shown on Figure 1. Fluid flows inwards in the circuit connected to the heat pump and outwards for the circuit connected to the solar collectors. This creates a counterflow heat exchanger within the bore field between the two circuits. The system includes a total of 22 components: 16 boreholes (1-16), a heat source (17) representing the heat pump, a heat source (18) representing the solar collectors, two flow splitters (19-20) and two flow mixer (21-22). The borehole length is H = 80 m for all boreholes. The nominal fluid mass flow rate of the circuit connected to the heat pump is 1.0 kg/s. The nominal fluid mass flow rate of the circuit connected to the solar collectors is 0.7 kg/s. Fluid flow is evenly distributed amongst the branches. As in the previous cases, when the heat pump is turned off or when no solar heat is stored, the mass flow rate of the associated circuit is reduced to 5% of its nominal value.

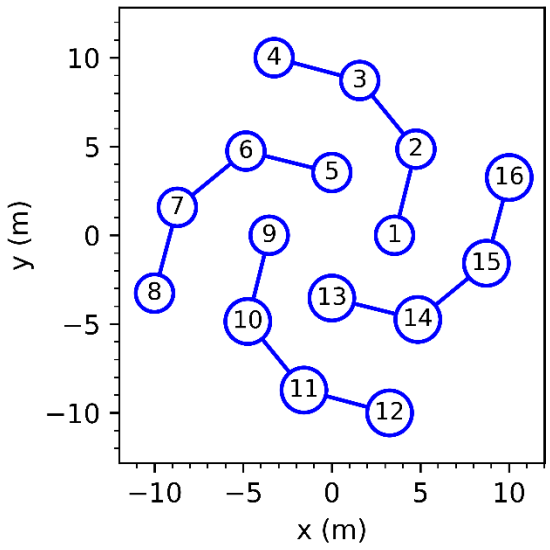

Figure 15. Position of boreholes in field of 16 boreholes with two independent fluid loops

Calculated average borehole wall temperatures and inlet and outlet fluid temperatures and the total heat extraction rate using the proposed method are presented in Figure 16 for hours 697-816 (5 weekdays, starting January 30th) of the 20th simulation year. During the 20th simulation year, the minimum fluid temperature is 0.44°C, the total heat extracted by the heat pump is 28,028 kWh, the total heat injected by the heat pump is 14,998 kWh and the total heat injected by the solar collectors is 39,987 kWh.

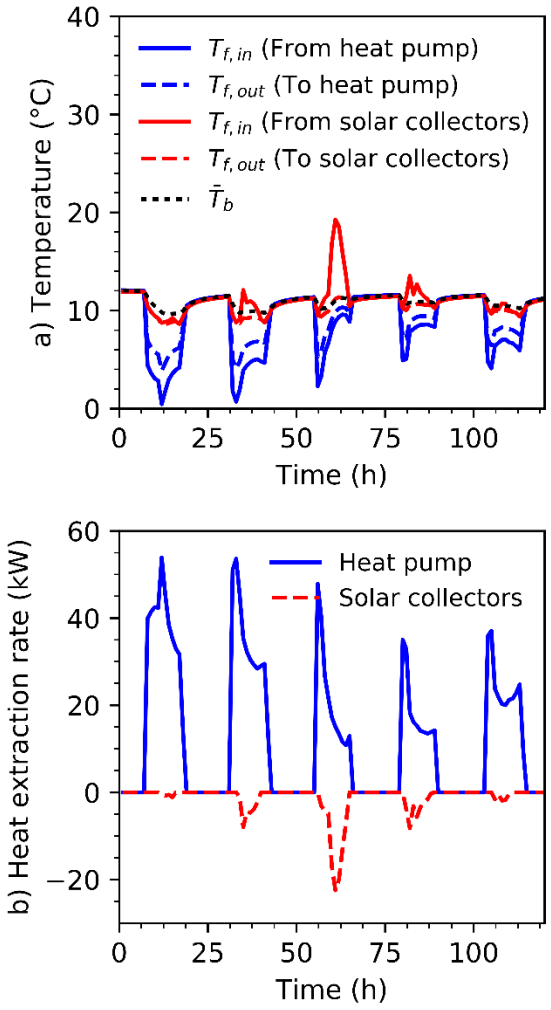

Figure 16. (a) Temperatures and (b) total heat extraction rates during five days of the 20th simulation year of the field of 16 parallel-connected boreholes with two independent fluid loops

The total simulation time using the presented methodology is 8,199 seconds, where 33 seconds is the computational time required for the initialization of the component models including the calculation of the segment-to-segment response factors, 3,153 seconds is the computational time required for the temporal superposition algorithm and 4,928 seconds is the computational time required for the solution of the coupled system-level heat and mass balance problems and the bore field heat transfer problem.

4. Discussion

The simulation times of all presented cases are summarized in Table 2. Note that the total of the times required for initialization, temporal superposition and the solution of the systems of equations does not amount to the total simulation time. Other operations, such as the evaluation of heat pump COP and solar collector efficiency, are not included in any of the three categories. Across the three given cases, the simulation time increased with two factors: the number of finite line sources per borehole and the number of evaluated matrix inverses in the systems of equations (Equations (37), (38) and (59)). The number of finite line source segments increases the size of the matrices related to the bore field heat transfer problem and thus the computational time needed for the matrix multiplications in the temporal superposition process (Equation (52)) and for the inversion of the matrix in Equation (59). While this increase in simulation time may seem significant, especially when compared to simulations using only 1 segment per borehole, it is important to note that the resulting system model is then fully discretized in space and accounts for the distribution of temperatures of the fluid and the ground and of the heat extraction rates along the length of the boreholes and from borehole to borehole.

Table 2 shows an important increase in the time required for temporal superposition with increasing number of segments in the bore field. For instance, temporal superposition in Case 1 using 12 segments per borehole (i.e. 192 segments total) takes 2,766 s of simulation time while Case 2 using 12 segments per borehole (i.e. 288 segments total) takes 10,263 s of simulation time. This indicates that simulation of systems with hundreds of boreholes will be very time consuming. Improved temporal superposition techniques are needed for the simulation of very large amounts of boreholes.

Table 2. Simulation times

Case	Initialization	Temporal superposition	System of equations	Total
Case 1 (12 segments)	15 s (0.3%)	2766 s (55%)	2186 s (43%)	5040 s
Case 1 (1 segment)	3 s (0.7%)	171 s (37%)	253 s (55%)	457 s
Case 2	41 s (0.3%)	10263 s (72%)	3847 s (27%)	14257 s
Case 3	33 s (0.4%)	3153 s (38%)	4928 s (60%)	8199 s

The matrix inverses in each of the systems of equations need to be evaluated whenever the coefficients in matrices $\boldsymbol{A}_{\dot{\boldsymbol{m}}_f}$, $\boldsymbol{A}_{\boldsymbol{T}_f}$ and $\boldsymbol{A}_{\boldsymbol{Q}_b}$ change. For the system component models presented in this paper, $\boldsymbol{A}_{\dot{\boldsymbol{m}}_f}$ only changes if the mass flow rate fractions in a splitter component change, $\boldsymbol{A}_{\boldsymbol{T}_f}$ changes if the mass flow rate fractions in a mixer component changes or if the mass flow rates in any borehole changes, and $\boldsymbol{A}_{\boldsymbol{Q}_b}$ changes if the mass flow rate in any borehole changes.

Alternate solution methods for the systems of linear equations might be preferred to the inversion of the matrices. Matrices for the system-level heat and mass balance problems have predictable sparse structures and can be stored in compressed form to allow for the simulation of very large systems. Off-diagonal terms in the segment-to-segment thermal response factor matrix $\boldsymbol{H}(\Delta t)$ can be neglected when the time step is sufficiently small, which is usually the case for hourly simulations. This also makes the matrix structure for the bore field heat transfer problem sparse.

5. Conclusion

A simulation model for geothermal systems with vertical boreholes is presented. Mathematical models are formulated for each of the system components, i.e. fluid sources and sinks, flow splitters and mixers, heat sources and vertical boreholes. System-level mass and heat balance problems are assembled from the formulated component-level mass and heat balance problems,

incorporating connections between component fluid outlets and inlets at the system level. A third problem is introduced for heat transfer in the bore field. The solution of the three problems yields the inlet and outlet fluid mass flow rates and temperatures, as well as the borehole wall temperatures and heat extraction rates.

The proposed simulation model is tested in three example systems. The first system is a field of 16 boreholes connected in parallel connected to a heat pump with temperature dependent COP. Simulation results from this first system are verified against a g-function based method. The second system adds 8 boreholes to the previous bore field. These additional boreholes are connected to flat plate solar collectors, with an efficiency dependent on fluid and ambient temperatures. The third system considers the case of 16 boreholes with two independent fluid loops running in counter flow in four parallel branches of four series-connected boreholes. In all three cases, heat extraction rates and fluid mass flow rates in the bore field are time-dependent. Due to solar heat injection into the ground in the second and third cases, the borehole length required to maintain fluid temperatures above 0°C was reduced from 115 m (i.e. 1,840 m total length) down to 85 m (i.e. 1,587 m total length) and 80 m (i.e. 1,280 m total length) in the second and third cases, respectively.

The presented model includes several notable contributions:

- Both fluid boundary conditions of specified fluid temperatures (through the fluid source component) and specified heating rate (through the heat source component) are possible.
- The simulation model allows for any kind of bore field arrangement (i.e. series, parallel and mixed) and any number of independent fluid loops.
- Boreholes can have different sizes in terms of length, buried depth and radius.

- The system-level (i.e. inlet and outlet fluid mass flow rates and temperatures) and bore field variables (i.e. borehole wall temperatures and heat extraction rates) are solved for in separate systems of equations of reduced size.
- Boreholes are divided into segments to consider the axial variation of fluid and borehole wall temperatures and heat extraction rates.

The presented model also presents many opportunities for future work. The presented borehole component model does not include the effects of the thermal capacity of the fluid and of the borehole materials. A short-time model of the borehole will be developed to be compatible with the presented model. The current mass balance problems do not account for head losses in the pipes to distribute flow between branches at the outlet of flow splitters and instead rely on user-specified flow fractions. A pipe network model will be developed to evaluate mass flow rates based on head loss calculations and coupled to the presented model. Finally, simulations of bore fields with large amounts of boreholes – and borehole segments – have very large simulation times. Improved temporal superposition algorithms will be developed to reduce simulation times.

Acknowledgements

The author received a start-up subsidy from the *Fonds de recherche du Québec – Nature et Technologie* (FRQNT).

References

Bauer, D., W. Heidemann, and H.-J.G. Diersch. 2011. “Transient 3D Analysis of Borehole Heat Exchanger Modeling.” *Geothermics* 40 (4): 250–260. doi:10.1016/j.geothermics.2011.08.001.

Belzile, P., L. Lamarche, and D. R. Rousse. 2016a. “Semi-Analytical Model for Geothermal

Borefields with Independent Inlet Conditions." *Geothermics* 60: 144–155. doi:10.1016/j.geothermics.2015.12.008.

Belzile, P., L. Lamarche, and D. R. Rousse. 2016b. "Geothermal Heat Exchange in Boreholes with Independent Sources." *Applied Thermal Engineering* 98: 1221–1230. doi:10.1016/j.applthermaleng.2015.12.028.

Bernier, M., P. Pinel, R. Labib, and R. Paillot. 2004. "A Multiple Load Aggregation Algorithm for Annual Hourly Simulations of GCHP Systems." *HVAC&R Research* 10 (4): 471–487. doi:10.1080/10789669.2004.10391115.

Cimmino, M. 2015. "The Effects of Borehole Thermal Resistances and Fluid Flow Rate on the g-Functions of Geothermal Bore Fields." *International Journal of Heat and Mass Transfer* 91: 1119–1127. doi:10.1016/j.ijheatmasstransfer.2015.08.041.

Cimmino, M. 2016. "Fluid and Borehole Wall Temperature Profiles in Vertical Geothermal Boreholes with Multiple U-Tubes." *Renewable Energy* 96: 137–147. doi:10.1016/j.renene.2016.04.067.

Cimmino, M., and M. Bernier. 2014. "A Semi-Analytical Method to Generate g-Functions for Geothermal Bore Fields." *International Journal of Heat and Mass Transfer* 70 (c): 641–650. doi:10.1016/j.ijheatmasstransfer.2013.11.037.

Cimmino, M., and P. Eslami-Nejad. 2016. "A Simulation Model for Solar Assisted Shallow Ground Heat Exchangers in Series Arrangement." *Energy and Buildings*. doi:10.1016/j.enbuild.2016.03.019.

Claesson, J., and G. Hellström. 2011. "Multipole Method to Calculate Borehole Thermal Resistances in a Borehole Heat Exchanger." *HVAC&R Research* 17 (6): 895–911. doi:10.1080/10789669.2011.609927.

Claesson, J., and S. Javed. 2011. "An Analytical Method to Calculate Borehole Fluid Temperatures for Time-Scales from Minutes to Decades." *ASHRAE Transactions* 117 (2): 279–288.

Claesson, J., and S. Javed. 2012. "A Load-Aggregation Method to Calculate Extraction Temperatures of Borehole Heat Exchangers." *ASHRAE Transactions* 118 (1): 530–539.

Cui, P., N. Diao, C. Gao, and Z. Fang. 2015. “Thermal Investigation of in-Series Vertical Ground Heat Exchangers for Industrial Waste Heat Storage.” *Geothermics* 57: 205–212. doi:10.1016/j.geothermics.2015.06.003.

Eskilson, P. 1987. “Thermal Analysis of Heat Extraction Boreholes.” University of Lund. Lund.

Eslami-nejad, P., and M. Bernier. 2011. “Coupling of Geothermal Heat Pumps with Thermal Solar Collectors Using Double U-Tube Boreholes with Two Independent Circuits.” *Applied Thermal Engineering* 31 (14–15): 3066–3077. doi:10.1016/j.applthermaleng.2011.05.040.

Hellström, G. 1991. “Ground Heat Storage: Thermal Analysis of Duct Storage Systems.” University of Lund. Lund.

Lamarche, L. 2009. “A Fast Algorithm for the Hourly Simulations of Ground-Source Heat Pumps Using Arbitrary Response Factors.” *Renewable Energy* 34 (10): 2252–2258. doi:10.1016/j.renene.2009.02.010.

Lamarche, L. 2017. “Mixed Arrangement of Multiple Input-Output Borehole Systems.” *Applied Thermal Engineering*. doi:10.1016/j.applthermaleng.2017.06.060.

Lamarche, L., and B. Beauchamp. 2007. “A New Contribution to the Finite Line-Source Model for Geothermal Boreholes.” *Energy and Buildings* 39 (2): 188–198. doi:10.1016/j.enbuild.2006.06.003.

Lamarche, L., S. Kajl, and B. Beauchamp. 2010. “A Review of Methods to Evaluate Borehole Thermal Resistances in Geothermal Heat-Pump Systems.” *Geothermics* 39 (2): 187–200. doi:10.1016/j.geothermics.2010.03.003.

Lazzarotto, A. 2014. “A Network-Based Methodology for the Simulation of Borehole Heat Storage Systems.” *Renewable Energy* 62: 265–275. doi:10.1016/j.renene.2013.07.020.

Lazzarotto, A. 2015. “Developments in Ground Heat Storage Modeling.” KTH Royal Institute of Technology. Stockholm.

Lazzarotto, A. 2016. “A Methodology for the Calculation of Response Functions for Geothermal Fields with Arbitrarily Oriented Boreholes – Part 1.” *Renewable Energy* 86: 1380–1393. doi:10.1016/j.renene.2015.09.056.

Lazzarotto, A., and F. Björk. 2016. “A Methodology for the Calculation of Response Functions

for Geothermal Fields with Arbitrarily Oriented Boreholes – Part 2." *Renewable Energy* 86: 1353–1361. doi:10.1016/j.renene.2015.09.057.

Liu, X. 2005. "Development and Experimental Validation of Simulation of Hydronic Snow Melting Systems for Bridges." Oklahoma State University. Stillwater.

Marcotte, D., and P. Pasquier. 2014. "Unit-Response Function for Ground Heat Exchanger with Parallel, Series or Mixed Borehole Arrangement." *Renewable Energy* 68: 14–24. doi:10.1016/j.renene.2014.01.023.

Monzó, P., J. Acuna, P. Mogensen, and B. Palm. 2013. "A Study of the Thermal Response of a Borehole Field in Winter and Summer." In *International Conference on Applied Energy*. Pretoria, South Africa. July 1-4, 2013.

Nguyen, A., P. Pasquier, and D. Marcotte. 2017. "Borehole Thermal Energy Storage Systems under the Influence of Groundwater Flow and Time-Varying Surface Temperature." *Geothermics* 66: 110–118. doi:10.1016/j.geothermics.2016.11.002.

Zarrella, A., G. Emmi, and M. De Carli. 2017. "A Simulation-Based Analysis of Variable Flow Pumping in Ground Source Heat Pump Systems with Different Types of Borehole Heat Exchangers: A Case Study." *Energy Conversion and Management* 131: 135–150. doi:10.1016/j.enconman.2016.10.061.

Zeng, H. Y., N. R. Diao, and Z. H. Fang. 2002. "A Finite Line-Source Model for Boreholes in Geothermal Heat Exchangers." *Heat Transfer - Asian Research* 31 (7): 558–567. doi:10.1002/htj.10057.

Appendix. Analytical borehole heat transfer model

The analytical model of Cimmino (Cimmino 2016) is adapted to calculate the coefficient matrices and vectors needed for the borehole component heat balance problem and the bore field heat transfer problem. This appendix describes the solution for the fluid temperatures and heat extraction rates in a borehole with independent U-tubes and an arbitrary borehole wall temperature profile.

The fluid temperature variations inside the borehole are driven by heat transfer between pipes and between individual pipes and the borehole wall. Steady-state heat conduction inside a borehole cross section can be represented as a network of delta-circuit thermal resistances, as shown on Figure A1. The total rate of heat transfer from a pipe i_p at a distance z from the top of the borehole is the sum of the rate of heat transferred to all other pipes and the borehole wall:

$$\dot{Q}_{p,i_b,i_p}(z) = \frac{T_{f,i_b,i_p}(z) - T_{b,i_b}(z)}{R^{\Delta}_{i_p,i_p}} + \sum_{\substack{j_p=1 \\ i_p \neq j_p}}^{2n_{p,i_b}} \frac{T_{f,i_b,i_p}(z) - T_{f,i_b,j_p}(z)}{R^{\Delta}_{i_p,j_p}} \qquad \text{(A1)}$$

where $\dot{Q}_{p,i_b,i_p}$ is the total rate of heat transfer from a pipe i_p inside borehole i_b, T_{f,i_b,i_p} is the fluid temperature inside pipe i_p of borehole i_b, T_{b,i_b} is the borehole wall temperature of borehole i_b, $R^{\Delta}_{i_p,i_p}$ is the delta-circuit thermal resistance between pipe i_p and the borehole wall and $R^{\Delta}_{i_p,j_p}$ is the delta-circuit thermal resistance between pipe i_p and pipe j_p.

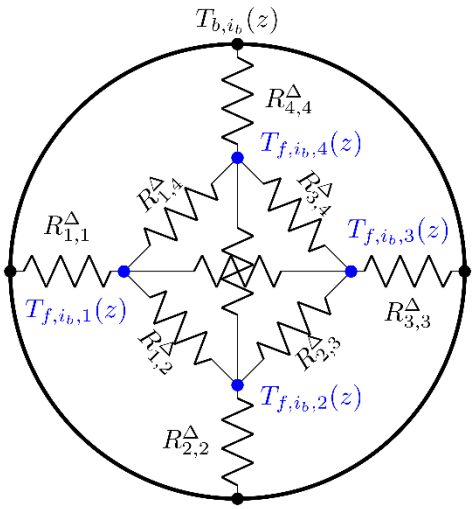

Figure A1. Delta-circuit of thermal resistances for a borehole with two U-tubes

The delta-circuit thermal resistances are dependent on the borehole geometry and thermal properties, i.e. the grout, ground, U-tube pipe material and fluid thermal conductivities, the

dimensions and position of the U-tube pipes inside the borehole, the borehole dimensions, and the convective thermal resistance between the fluid and the inner pipe walls. These delta-circuit thermal resistances can be evaluated by means of analytical methods such as the multipole method (Claesson and Hellström 2011) and the line source approximation (Hellström 1991). Other analytical and numerical methods have been reviewed by Lamarche et al. (Lamarche, Kajl, and Beauchamp 2010). In the context of this paper, delta-circuit thermal resistances are calculated using the line source approximation.

From thermal energy balances on each of the pipes at a cross-section z, a linear system of differential equations is built for the fluid temperatures along the pipes with an arbitrary borehole wall temperature along the borehole:

$$\frac{\partial \boldsymbol{T}_{f,\boldsymbol{i_b}}}{\partial z}(z) = \boldsymbol{A}_{\boldsymbol{i_b}} \boldsymbol{T}_{f,\boldsymbol{i_b}}(z) - \boldsymbol{A}_{\boldsymbol{i_b}} \mathbf{1}_{2n_{p,i_b}\times 1} T_{b,i_b}(\mathrm{z}),\ 0 \le z \le H_{i_b} \tag{A2}$$

$$\boldsymbol{A}_{\boldsymbol{i_b}} = \begin{bmatrix} A_{i_b,1,1} & \cdots & A_{i_b,1,2n_{p,i_b}} \\ \vdots & \ddots & \vdots \\ A_{i_b,2n_{p,i_b},1} & \cdots & A_{i_b,2n_{p,i_b},2n_{p,i_b}} \end{bmatrix} \tag{A3}$$

$$A_{i_b,i_p,j_p} = \begin{cases} \dfrac{-1}{\dot{m}_{f,in,i_b,i_p} c_{p,i_b,i_p}} \sum_{j_p=1}^{2n_{p,i_b}} \dfrac{1}{R^{\Delta}_{i_p,j_p}} & i_p = j_p \quad i_p \le n_{p,i_b} \\ \dfrac{1}{\dot{m}_{f,in,i_b,i_p} c_{p,i_b,i_p} R^{\Delta}_{i_p,j_p}} & i_p \ne j_p \quad i_p \le n_{p,i_b} \\ \dfrac{1}{\dot{m}_{f,in,i_b,i_p} c_{p,i_b,i_p}} \sum_{j_p=1}^{2n_{p,i_b}} \dfrac{1}{R^{\Delta}_{i_p,j_p}} & i_p = j_p \quad i_p > n_{p,i_b} \\ \dfrac{-1}{\dot{m}_{f,in,i_b,i_p} c_{p,i_b,i_p} R^{\Delta}_{i_p,j_p}} & i_p \ne j_p \quad i_p > n_{p,i_b} \end{cases} \tag{A4}$$

where $\boldsymbol{T}_{\boldsymbol{f},\boldsymbol{i_b}}$ is a $2n_{p,i_b} \times 1$ column vector of fluid temperatures in all pipes of borehole i_b and c_{p,i_b,i_p} is the specific heat capacity of the fluid circulating in pipe i_p of borehole i_b.

The analytical solution to Equation (A2) is given by the matrix exponential of $\left(\boldsymbol{A}_{i_b} z\right)$ (Cimmino 2016). Assuming a piecewise uniform borehole wall temperature over borehole segments of equal length, where $T_{b,i_b,u}$ is the temperature along the u-th segment of borehole i_b (i.e. over the portion $(u-1)H_{i_b}/n_{q,i_b} \leq z < uH_{i_b}/n_{q,i_b}$) and n_{q,i_b} is the number of borehole segments for borehole i_b, the fluid temperatures at any depth z of borehole i_b are given by:

$$\boldsymbol{T}_{\boldsymbol{f},\boldsymbol{i_b}}(z) = \boldsymbol{E}_{\boldsymbol{i_b}}(z)\begin{bmatrix}\boldsymbol{T}_{\boldsymbol{f},\boldsymbol{in},\boldsymbol{i_b}} \\ \boldsymbol{T}_{\boldsymbol{f},\boldsymbol{out},\boldsymbol{i_b}}\end{bmatrix} - \boldsymbol{F}_{\boldsymbol{i_b}}(z)\boldsymbol{T}_{\boldsymbol{b},\boldsymbol{i_b}} \tag{A5}$$

$$\boldsymbol{E}_{\boldsymbol{i_b}}(\mathrm{z}) = \exp\left(\boldsymbol{A}_{\boldsymbol{i_b}} z\right) = \boldsymbol{V}_{\boldsymbol{i_b}} \exp\left(\boldsymbol{L}_{\boldsymbol{i_b}} z\right) \boldsymbol{V}_{\boldsymbol{i_b}}^{-1} \tag{A6}$$

$$\boldsymbol{F}_{\boldsymbol{i_b}}(\mathrm{z}) = \begin{bmatrix}\boldsymbol{F}_{\boldsymbol{i_b},\boldsymbol{1}}(\mathrm{z}) & \cdots & \boldsymbol{F}_{\boldsymbol{i_b},\boldsymbol{n_{q,i_b}}}(\mathrm{z})\end{bmatrix} \tag{A7}$$

$$\boldsymbol{F}_{\boldsymbol{i_b},\boldsymbol{u}}(\mathrm{z}) = \boldsymbol{V}_{\boldsymbol{i_b}}\boldsymbol{L}_{\boldsymbol{i_b}}^{-\boldsymbol{1}}\left[\exp\left(\boldsymbol{L}_{\boldsymbol{i_b}}\left(z - \min\left(z, \frac{(u-1)H_{i_b}}{n_{q,i_b}}\right)\right)\right) - \exp\left(\boldsymbol{L}_{\boldsymbol{i_b}}\left(z - \min\left(z, \frac{uH_{i_b}}{n_{q,i_b}}\right)\right)\right)\right]\boldsymbol{V}_{\boldsymbol{i_b}}^{-1}\boldsymbol{A}_{\boldsymbol{i_b}}\boldsymbol{1}_{2n_{p,i_b}\times 1} \tag{A8}$$

where $\boldsymbol{E}_{\boldsymbol{i_b}}(\mathrm{z})$ is the matrix exponential of $\boldsymbol{A}_{\boldsymbol{i_b}} z$, $\boldsymbol{V}_{\boldsymbol{i_b}}$ is the matrix of column eigenvectors of $\boldsymbol{A}_{\boldsymbol{i_b}}$, $\boldsymbol{L}_{\boldsymbol{i_b}}$ is a diagonal matrix with the eigenvalues of $\boldsymbol{A}_{\boldsymbol{i_b}}$ along the diagonal and $\mathrm{ceil}(x)$ is the ceiling rounded value of x.

By imposing equal fluid temperatures at the bottom of the U-tubes (i.e. $T_{f,i_b,i_p}\left(H_{i_b}\right) = T_{f,i_b,i_p+n_{p,i_b}}\left(H_{i_b}\right)$), the relation between inlet and outlet fluid temperatures is given by:

$$\boldsymbol{E}_{\boldsymbol{out},\boldsymbol{i_b}}\left(H_{i_b}\right)\boldsymbol{T}_{\boldsymbol{f},\boldsymbol{out},\boldsymbol{i_b}} = \boldsymbol{E}_{\boldsymbol{in},\boldsymbol{i_b}}\left(H_{i_b}\right)\boldsymbol{T}_{\boldsymbol{f},\boldsymbol{in},\boldsymbol{i_b}} + \boldsymbol{E}_{\boldsymbol{b},\boldsymbol{i_b}}\left(H_{i_b}\right)\boldsymbol{T}_{\boldsymbol{b},\boldsymbol{i_b}} \tag{A9}$$

$$\boldsymbol{E_{in,i_b}}(z) = \left[-\boldsymbol{I}_{n_{p,i_b}}, \boldsymbol{I}_{n_{p,i_b}}\right] \boldsymbol{E_{i_b}}(\mathrm{z}) \begin{bmatrix} \boldsymbol{I}_{n_{p,i_b}} \\ \boldsymbol{0}_{n_{p,i_b} \times n_{p,i_b}} \end{bmatrix} \tag{A10}$$

$$\boldsymbol{E_{out,i_b}}(z) = \left[\boldsymbol{I}_{n_{p,i_b}}, -\boldsymbol{I}_{n_{p,i_b}}\right] \boldsymbol{E_{i_b}}(\mathrm{z}) \begin{bmatrix} \boldsymbol{0}_{n_{p,i_b} \times n_{p,i_b}} \\ \boldsymbol{I}_{n_{p,i_b}} \end{bmatrix} \tag{A11}$$

$$\boldsymbol{E_{b,i_b}}(\mathrm{z}) = \left[\boldsymbol{I}_{n_{p,i_b}}, -\boldsymbol{I}_{n_{p,i_b}}\right] \boldsymbol{F_{b,i_b,u}}(\mathrm{z}) \tag{A12}$$

The heat extraction rate of a segment u of a borehole i_b can be obtained from a thermal energy balance on the fluid:

$$\dot{Q}_{b,i_b,u} = [\boldsymbol{M_{i_b}} \quad -\boldsymbol{M_{i_b}}] \left[\boldsymbol{T_{f,i_b}}\left(\frac{uH_{i_b}}{n_{q,i_b}}\right) - \boldsymbol{T_{f,i_b}}\left(\frac{(u-1)H_{i_b}}{n_{q,i_b}}\right)\right] \tag{A13}$$

$$\boldsymbol{M_{i_b}} = \left[\dot{m}_{f,in,i_b,1} c_{p,i_b,1} \quad \cdots \quad \dot{m}_{f,in,i_b,n_p} c_{p,i_b,n_p}\right] \tag{A14}$$

From Equations (A5) and (A9), the fluid temperatures at any depth can be expressed as a function of the inlet fluid temperatures and the borehole wall temperatures:

$$\boldsymbol{T_{f,i_b}}(z) = \boldsymbol{E_{i_b}}(z) \begin{bmatrix} \boldsymbol{I}_{n_{p,i_b}} \\ \boldsymbol{E_{out,i_b}^{-1}}(H_{i_b}) \boldsymbol{E_{in,i_b}}(H_{i_b}) \end{bmatrix} \boldsymbol{T_{f,in,i_b}} + \left(\boldsymbol{E_{i_b}}(z) \begin{bmatrix} \boldsymbol{0}_{n_{p,i_b} \times n_{p,i_b}} \\ \boldsymbol{E_{out,i_b}^{-1}}(H_{i_b}) \boldsymbol{E_{b,i_b}}(H_{i_b}) \end{bmatrix} - \boldsymbol{F_{i_b}}(z) \right) \boldsymbol{T_{b,i_b}} \tag{A15}$$

From Equation (A15) and the aforementioned thermal energy balance (Equation (A13)), the heat extraction rates can be expressed as a function of inlet fluid temperatures and borehole wall temperatures:

$$\dot{\boldsymbol{Q}}_{\boldsymbol{b},\boldsymbol{i_b}}(t_k) = -\boldsymbol{\Delta F}_{\boldsymbol{i_b}}\boldsymbol{T}_{\boldsymbol{b},\boldsymbol{i_b}}(t_k) + \boldsymbol{\Delta E}_{\boldsymbol{i_b}}\begin{bmatrix} \boldsymbol{I}_{n_{p,i_b}} \\ \boldsymbol{E}_{\boldsymbol{out},\boldsymbol{i_b}}^{-1}(H_{i_b})\boldsymbol{E}_{\boldsymbol{in},\boldsymbol{i_b}}(H_{i_b}) \end{bmatrix}\boldsymbol{T}_{\boldsymbol{f},\boldsymbol{in},\boldsymbol{i_b}} \quad \text{(A16)}$$

$$\boldsymbol{\Delta F}_{\boldsymbol{i_b}} = \begin{bmatrix} \boldsymbol{\Delta F}_{\boldsymbol{i_b},\boldsymbol{1}} \\ \vdots \\ \boldsymbol{\Delta F}_{\boldsymbol{i_b},\boldsymbol{n_{q,i_b}}} \end{bmatrix} \quad \text{(A17)}$$

$$\boldsymbol{\Delta F}_{\boldsymbol{i_b},\boldsymbol{u}} = [\boldsymbol{M}_{\boldsymbol{i_b}} \quad -\boldsymbol{M}_{\boldsymbol{i_b}}]\left[\boldsymbol{F}_{\boldsymbol{i_b}}\left(\frac{uH_{i_b}}{n_{q,i_b}}\right) - \boldsymbol{F}_{\boldsymbol{i_b}}\left(\frac{(u-1)H_{i_b}}{n_{q,i_b}}\right)\right] \quad \text{(A18)}$$

$$\boldsymbol{\Delta E}_{\boldsymbol{i_b}} = \begin{bmatrix} \boldsymbol{\Delta E}_{\boldsymbol{i_b},\boldsymbol{1}} \\ \vdots \\ \boldsymbol{\Delta E}_{\boldsymbol{i_b},\boldsymbol{n_{q,i_b}}} \end{bmatrix} \quad \text{(A19)}$$

$$\boldsymbol{\Delta E}_{\boldsymbol{i_b},\boldsymbol{u}} = [\boldsymbol{M}_{\boldsymbol{i_b}} \quad -\boldsymbol{M}_{\boldsymbol{i_b}}]\left[\boldsymbol{E}_{\boldsymbol{i_b}}\left(\frac{uH_{i_b}}{n_{q,i_b}}\right) - \boldsymbol{E}_{\boldsymbol{i_b}}\left(\frac{(u-1)H_{i_b}}{n_{q,i_b}}\right)\right] \quad \text{(A20)}$$